Flow past a rotationally oscillating cylinder near a plane wall

Soumarup Bhattacharyya,[*] Raghavendra Naidu S,[†] Kamal Poddar,[‡] and Sanjay Kumar[§]
Department of Aerospace Engineering, Indian Institute of Technology Kanpur, Kanpur, UP-208016, India

(Received 30 January 2023; accepted 28 August 2023; published 27 September 2023)

The wake of a rotationally oscillating cylinder in the presence of a plane wall with various gap-to-diameter ratios are studied experimentally for a Reynolds number of 250. Flow visualization study is conducted using planar laser-induced fluorescence and hydrogen bubble technique in the plane perpendicular to the cylinder and in the spanwise plane, respectively, to find the effect of gap distance on the wake structures for various forcing frequencies and amplitudes. Quantitative analysis is provided using hot-wire anemometry to find the lock-on parameter space and particle image velocimetry (PIV) revealed the strength of vortices shed perpendicular to the cylinder. Various wake structures, like single-sided shedding, double-layer vortices, and detached shear layer shedding from the wall, are observed for different gap distances and forcing parameters using laser-induced fluorescence flow visualizations. PIV data reveals that the circulation strength of the vortices shed perpendicular to the cylinder reduces with increasing downstream distance. Hot-wire analysis reveals one of the key outcomes of the study, showing that the range of frequency-amplitude parameter space for which the lock-on phenomenon occurs reduces with a decrease in wall distance. Hydrogen bubble flow visualization data reveal the presence of two spanwise three-dimensional modes and characteristics of these modes with varying forcing conditions and gap distance are found. Interestingly, it is observed that there is a lack of three-dimensionalities in the flow when the gap ratio (wall spacing-to-diameter ratio) is reduced to $G/D = 0.5$.

DOI: 10.1103/PhysRevFluids.8.094102

I. INTRODUCTION

The fluid flow characteristics around circular cylinders in the presence of a wall have been extensively studied in recent decades (Price *et al.* [1], Grass *et al.* [2], etc.). The planar boundary affects the flow physics of the wake behind the oscillating cylinder and affects the Strouhal number, the transition regime, and the drag on the cylinder. This study may have practical engineering applications in offshore (the behavior of pipeline risers near the touchdown zone Bridge *et al.* [3]) and underwater engineering, fluid mixing during chemical spilling (Ivshina *et al.* [4]) and military applications such as submarine homing. Another interesting application of this study may be in industrially important devices like tube-bank heat exchangers where the presence of a wall may affect the vortex-induced vibrations (Sellapan and Pottebaum [5]). In practical applications involving fluid mixing, it is very likely that multiple cylinders will be used. A recent study by

[*]Presently at Department of Naval Architecture and Marine Engineering, University of Michigan, Ann Arbor 48109, USA; soumarup@umich.edu
[†]srnaidu@iitk.ac.in
[‡]kamal@iitk.ac.in
[§]Corresponding author: skmr@iitk.ac.in

Izhar Hussain *et al.* [6] involves investigating flow characteristics past two rotationally oscillating cylinders. These problems are inherently complex involving several control parameters. The study reported in the present work on rotationally oscillating cylinder near a plane wall serves as a canonical problem for more complex configurations involving forced cylinders near a plane wall. These flows are characterized by the Reynolds number, Re, defined as $\mathrm{Re} = DU_\infty/\nu$, where D is the cylinder diameter; U_∞ is the free-stream velocity; ν is the kinematic viscosity; and the gap ratio, G/D, is defined as the ratio between the cylinder-wall distance and the cylinder diameter.

Taneda [7] first reported vortex street of a single row formed behind the stationary cylinder confined near a planar boundary instead of regular Kármán vortices at $\mathrm{Re} = 170$. Bearman and Zdravkovich [8] through hot-wire measurements showed that there is suppression of vortex shedding at $G/\mathrm{D} \leqslant 0.3$ for a stationary cylinder at $\mathrm{Re} = 45000$. This study also revealed that the separation point travels downstream as G/D is reduced and the critical gap height is sensitive to upstream flow conditions. Grass *et al.* [2] observed that the magnitude of the separation pressure on the bottom face of the cylinder decreases as the gap height decreases and suggested that the suppression mechanism for the stationary cylinder is more explicitly related to viscous wall effects and the generation of opposite sign vorticity on the wall. Below the range of $0.35 \leqslant G/D \leqslant 0.5$, the shedding is completely suppressed and, above it, shedding takes place at all times. Lei *et al.* [9] suggested through pressure measurements that the critical value for vortex suppression is $G/D = 0.3$; Reynolds number effects on the critical value of G/D for which suppression occurs was studied numerically with finite difference method by Lei *et al.* [10]. For the present study, the minimum G/D is 0.5, where shedding is not suppressed, as the main purpose of the investigation is to find the interaction of shed vortices and the wall boundary layer. Finding the critical G/D for which the shedding occurs is not a part of the present work.

Zdravkovich [11] observed that the drag coefficient was unaffected until G/D was comparable to boundary layer thickness but the lift coefficient was greatly affected by the G/D. The Strouhal number, St (defining the vortex shedding frequency), increases progressively as the gap distance(G/D) is reduced below two cylinder diameters. The St can increase up to 25% at a critical G/D ratio where vortex shedding suppression begins (Grass *et al.* [2]). Measurements with the help of a stopwatch at $\mathrm{Re} = 500$ revealed that the St remains constant at 0.2 after $G/D \geqslant 2$ and reaches up to 0.252 at $G/D = 0.625$ (Cheng *et al.* [12]). Lei *et al.* [9] confirmed that the maximum St occurs at $G/D = 0.65$. Hot film and PIV (particle image velocimetry) experiments at $1200 \leqslant \mathrm{Re} \leqslant 4960$ revealed that there is no separation of the wall boundary layer either upstream or downstream for $G/D \geqslant 1$ (Price *et al.* [1]). Hence, after a certain gap-ratio, separation bubble does not appear because of the cancellation of vorticity on the side of the cylinder near the wall. Dipankar and Sengupta [13] through numerical stability analysis observed that with increasing gap-ratio, the adverse pressure gradient weakens, and for higher gap-ratio, separation upstream of the cylinder is weak. An important conclusion drawn from this study was that the instability is mainly determined by the gap and originates from the surface of the cylinder and not the wall.

There have been some studies where the wake of the cylinder close to the wall is controlled by using certain forcing parameters. These include rotation of the cylinder or imparting rotational oscillation to the cylinder. Cheng and Luo [14] simulated a two-dimensional flow around a rotating circular cylinder near a planar boundary by using the lattice Boltzmann equation with multiple relaxation times at Reynolds number $\mathrm{Re} = 200$. It was observed that the lift and drag exerted on the cylinder depended on the gap as well as the rotation rate. When the gap is small, the wall exerts greater influence on the lift and drag forces for a rotating cylinder than a stationary one. Recent wake research by Chikkam and Kumar [15] showed the influence of α and hydrophobicity on the wake structure of a hydrophobic spinning cylinder at $\mathrm{Re} \approx 200$. Taneda [7] experimentally studied wake structures of flow past a rotationally oscillating circular cylinder using flow visualization methods in the $\mathrm{Re} = 30$ to $\mathrm{Re} = 300$ range. Oscillation amplitudes ranged from $\pi/6$ to $\pi/2$ and a wide range of forcing frequencies were used. Since then, there have been several two-dimensional studies on the

wake of a rotationally oscillating isolated cylinder for various forcing frequencies and amplitudes, the relatively recent being Thiria *et al.* [16] and Kumar *et al.* [17]. The wake of a rotationally oscillating cylinder can potentially develop three-dimensional characteristics, thus altering drag, which depends upon the forcing frequency and amplitude of oscillation (Thiria and Wesfreid [18]). Lu and Sato. [19] observed using two-dimensional computations at Re = 200, 1000, and 3000 that the large-scale modes near the cylinder were not strongly affected by the Reynolds number. Kumar *et al.* [17] reported the flow visualization data for various forcing parameters at Re = 185 and also showed that for certain forcing parameters the flow turns three-dimensional. Conditions of lock-on, where oscillation frequency matches with the shedding frequency in the wake, were identified in the study. The primary motivation of the present study is to find out the effect of this lock-on phenomenon and the wake structure due to instabilities at similar forcing conditions when the cylinder is confined to a planar wall at various gap distances. Sunil *et al.* [20] recently performed experimental research on a rotationally oscillating cylinder with a flexible filament. Similar diagnostics are carried out in the current investigation using planar PIV to characterize the velocity and vorticity field.

Wake three-dimensionalities initiate a transition to turbulence and have important engineering significance. The study of wake three-dimensionalities around a stationary circular cylinder without a planar boundary has been reviewed comprehensively in the review article of Williamson [21]. The transition regime first observed by Roshko [22] was studied experimentally and was seen to involve two discontinuous modes by Williamson [23]. These two three-dimensional modes, namely Mode *A* and Mode *B*, develop after Re $\approx$ 190 where double-row vortices serve as a base flow. The presence of these modes was confirmed numerically by Dusek *et al.* [24], Barkley and Henderson [25], and Thompson *et al.* [26] and experimentally by Zhang *et al.* [27], Wu *et al.* [28], and Leweke and Williamson [29]. Three-dimensional modes in the wake of a rotating isolated cylinder have been studied numerically by Rao *et al.* [30] and the same has been validated experimentally by Radi *et al.* [31]. Three new modes other than Mode *A* (large-scale disturbances) and Mode *B* (small-scale disturbances) for stationary cylinders have been observed by Radi *et al.* [31] and these instabilities were characterized by their spanwise wavelength, structures, and motion of the disturbances. Recently, Bhattacharyya *et al.* [32] revealed three-dimensional characteristics of the wake of an isolated rotationally oscillating cylinder at Re = 250 and this study serves as the motivation to find if these three-dimensional wake structures are affected by a planar wall kept at different distances from the cylinder. Floquet stability analysis at Re = 300 by Lo Jacono *et al.* [33] with similar forcing conditions showed that in spite of the suppression of three-dimensional modes (Mode *A* and Mode *B*) another mode with spatiotemporal symmetry as Mode *A* is observed which renders the flow three-dimensional (named as Mode *D* in their study).

The present experiments consist of two-dimensional (*xz* plane) and three-dimensional (*xy* plane) studies pertaining to the wall effect on the flow downstream (near to intermediate wake distance) of a rotationally oscillating cylinder. The important questions that would be answered through this study are the following: (i) How does the planar boundary affect the flow behind the rotationally oscillating cylinder? (ii) What are the forcing parameters (amplitude and forcing frequency) for which we find new three-dimensional modes? (iii) What are the effects of forcing parameters on two-dimensional and three-dimensional wake structures? (iv) How is the lock-on affected by the forcing of the flow and changing of the gap distance?

The answer to these questions will provide some qualitative and quantitative insights into the cylinder vortex shedding modes in the presence of a planar boundary. More specifically, it will provide insight into the evolution of new three-dimensional modes in the spanwise (*xy*) plane. This will help to address some of the fundamental issues of boundary-layer effects in cylinder wakes such as the evolution of modes that are coherent and incoherent with space and time under forcing. This study would also provide an understanding of the development or suppression of three-dimensional modes which eventually aid the flow to become turbulent.

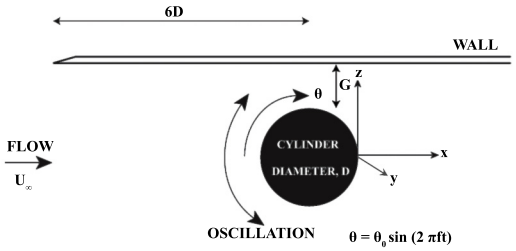

FIG. 1. Schematic of the problem.

II. EXPERIMENTAL SETUP AND VALIDATION

A. Experimental setup

The experiments for the present study are performed in a close circuit, free surface water tunnel (Rolling Hills Inc., Model 0710) in the Fluid Dynamics Laboratory, Indian Institute of Technology, Kanpur. The test section has a length of 0.46 m, a width of 0.18 m, and a depth of 0.25 m. The water velocity required to achieve Re = 250 and Re = 190 is $u \approx 0.03125$ m/s and $u \approx 0.02375$ m/s, respectively, in the present study. The schematic of the problem is shown in Fig. 1. The vortex-shedding frequency of the stationary cylinder is denoted by f_0. The frequencies in the present study are all nondimensionalized using f_0. The ratio f/f_0 is called the frequency ratio and is denoted by FR. The cylinder was forced to oscillate according to

$$\theta = \theta_0 \sin(2\pi f t), \tag{1}$$

where θ is the angular position of the cylinder, θ_0 is the oscillation amplitude, f is the forcing frequency, and t is time.

A rectangular glass piece of size 0.470 m × 0.175 m × 0.03 m, with a wide slot in the middle to accommodate a ball bearing through which the cylinder was rotationally oscillated, was placed on top of the test section. At the time of the experiments, the water surface was touching the glass. The experimental setup for laser-induced fluorescence flow visualization in the xz plane is schematically shown in Fig. 2. The cylinder was connected to a servo motor using a timing pulley and belt mechanism to ensure minimum wobbling and was inserted from above midway between the two tunnel sidewalls through the slot. It spanned the full depth of the tunnel. The tunnel floor was a black anodized chamfered aluminum plate with a bearing in it to hold the cylinder from the bottom. The cylinder used in the experiments was a stainless steel rod of length 0.270 m and diameter 0.008 m. The aspect ratio based on the cylinder's wetted length was 30. The motor was linked to a servo motor drive (M2DV-3D02R by Shanghai Moons Electric Co. Ltd.) and was controlled by a workstation using the motor software (M Servo Suite). A signal generator (model DG 1000) from Rigol, which provided sinusoidal analog signals of known frequency, was also coupled to the motor. This signal controlled the frequency of oscillation of the cylinder.

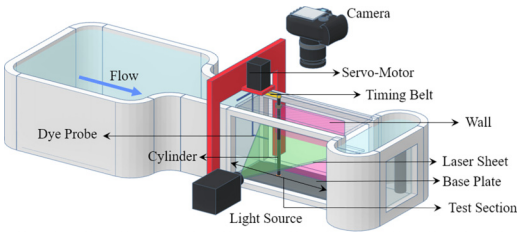

FIG. 2. Schematic of the experimental setup for laser-induced fluorescence flow visualization in xz plane.

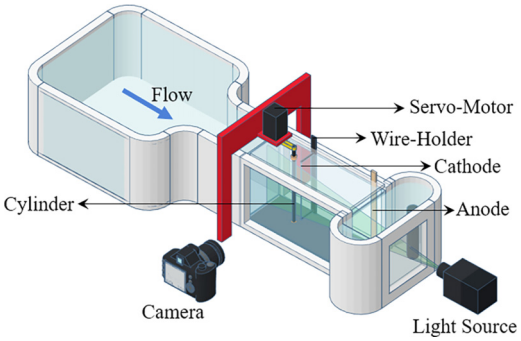

FIG. 3. Schematic of the experimental setup for hydrogen-bubble flow visualization in *xy* plane. The case of isolated cylinder is shown for clarity.

The wall was a 0.010-m-thick perplex sheet mounted at various gaps from the cylinder. It had a length of 0.32 m and it covered a streamwise distance of 6D upstream of the cylinder to 33D downstream of the cylinder. The leading edge of the plate was chamfered to prevent vortex shedding from the plate. The flow visualization was performed using the hydrogen bubble flow visualization (HBF) technique and the laser-induced fluorescence (LIF) technique. While experimenting it was found that the LIF technique for flow visualization produced better results for visualization in the *xz* plane. In the LIF technique rhodamine dye was injected with dye probes positioned 7D upstream of the cylinder. One dye probe was placed behind the cylinder and the other dye probe was kept near the wall to visualize the wall effect. The dye probe was significantly smaller (1/10D) as compared to the cylinder diameter and hence did not affect the shedding process. All the visualization data with LIF are presented with the flow directed from left to right and the wall at the top of all the frames. The HBF visualization was more suitable for the visualization in the *xy* plane. The HBF flow visualization was performed with a 50 μm diameter platinum wire kept in the spanwise plane, acting as the cathode, and a brass plate, acting as an anode, placed 390 mm downstream. A potential difference of ≈8.5–12.5 V was effective in obtaining good quality hydrogen bubbles. A small amount (≈30–35 g) of sodium sulfate was added to the water in the tunnel to facilitate electrolysis and improve the quality of hydrogen bubbles. The hydrogen bubbles formed on the platinum wire are swept downstream by the flow to form a sheet of bubbles. The continuous laser is used from the end of the tunnel to illuminate the bubbles for hydrogen bubble flow visualization. The bubbles form bright streaks when they cross the laser sheet. The experimental setup for hydrogen bubble flow visualization in the 3D view is shown in Fig. 3. The case of an isolated cylinder is shown for clarity and for the cases with the planar boundary, the wall is placed on the side of the cylinder opposite to that of the side where the platinum wire is placed. The flow structures in both the planes made visible by the illuminated bubble sheet or dye were captured with a Nikon D810 digital video recorder and viewing perpendicular to the illumination. Motion pictures are obtained at 60 fps and all of the experiments are done with ISO and focal length adjusted to get a clear good quality of image recording. The framing rate of the video camera provided a good resolution to characterize the flow structures at relatively low Reynolds numbers (190 and 250) in the present experiments. The visualization data that are presented in this present work are essentially at the same phase corresponding to the maximum angular displacement from the origin in the clockwise direction when viewed from the top.

The frequency content of the wake of the oscillating cylinder in the presence of the planar wall was measured by means of hot-film anemometry using a single sensor fiber-film probe. A Dantec miniCTA 54T42 system is used for acquiring spectral data. The probe was mounted on a straight holder with the help of an XY traverse. The data is acquired using a NI-9125 at a resolution of 16 bits, with a sampling rate of 1000 samples per second for 30 s for determining the shedding

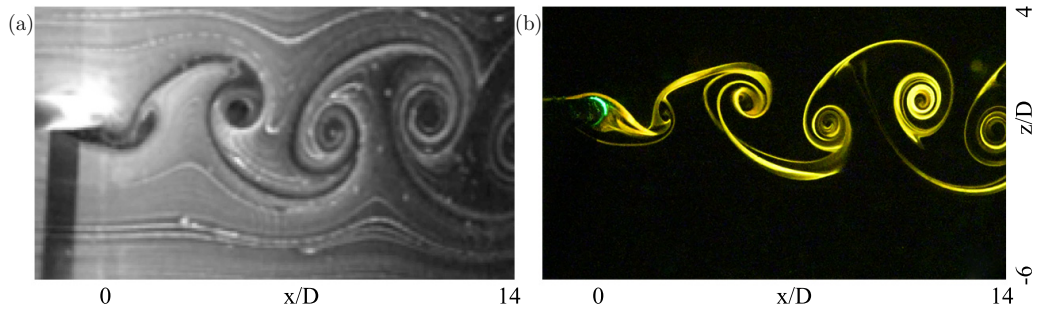

FIG. 4. Validation of the experimental setup for flow visualization in xz plane; (a) Kumar *et al.* [17], (b) present experiment without wall. The forcing parameters for both the cases are FR $= 0.8$ and $\theta_0 = \pi/2$. Flow is directed from left to right at Re $= 190$ and scaling is same for both the images.

frequency of the stationary cylinder. There was a good agreement of Re-St variation data from $190 \leqslant \text{Re} \leqslant 250$ where three dimensionalities of a stationary isolated cylinder (without wall) are prominent. The shedding frequency of the stationary cylinder f_0 was observed to be ≈ 0.74 Hz and 0.53 Hz at Re $= 250$ and Re $= 190$ respectively and this value would be further used for the calculation of nondimensional forcing frequency, FR.

The flow uniformity was inspected both by using hot-wire anemometry and particle image velocimetry (PIV). The hot-wire sensor was placed at a 4D location downstream of the cylinder for finding the Strouhal number. The spanwise wavelength of modes in three-dimensional flow cases from the digital images was obtained by drawing a straight line across the spanwise length and finding the pixel intensity along it to find the spanwise wavelength. The dominant peak in the FFT of the intensity profile denoted the spanwise wavelength of the mode.

PIV measurements were performed in the water tunnel in the same experimental conditions (but as different realizations) as the flow visualization experiments. The light source and camera were a pulsed laser (instead of a continuous laser used for flow visualization) and a PIV camera (instead of the Nikon Camera used for flow visualization), respectively. A TSI PIV system using the TSI Insight 4G platform was used to control the camera and firing of the laser to capture the images. The flow was seeded with 10 μm diameter hollow glass spheres by Dantec Dynamics and illuminated in a horizontal plane downstream of the cylinder with a laser sheet. The laser sheet was obtained by using the cylindrical lens optics placed in front of the double-pulsed Quantel Evergreen laser (532 nm–300 mJ/pulse). The laser sheet was focused down to a thickness of less than a millimeter near the cylinder's spanwise location. The digital image data of the glass spheres (particles) in the plane of the laser sheet are obtained using a TSI Powerview Plus 8MP CCD camera for further analysis. The size of the captured images was 2334×1751 pixels and the physical domain of the images was 170 mm $\times$ 130 mm, corresponding to a magnification of about 0.052 mm/pixel. The image processing was performed using 32×32 interrogation areas with 50% overlap in both the horizontal and vertical directions. This resulted in a spatial resolution of 1.664 mm (32 pixels $\times$ 0.052 mm/pixel) or 0.208 D in the vorticity fields of the present data. The camera and the laser pulse were synchronized using a synchronizer. The free-stream turbulence intensity was 3–4% in the present experimental conditions. Frame independence test for phase-locked time-averaged PIV of 100 frames and 400 frames showed identical results.

B. Validation

Validation of the experimental setup using flow visualization in xz plane with Kumar *et al.* [17] was performed. One such comparison at FR $= 0.8$ and $\theta_0 = \pi/2$ using LIF flow visualization is presented in Fig. 4. The flow in this case is characterized by the periodic, Kármán-like vortex

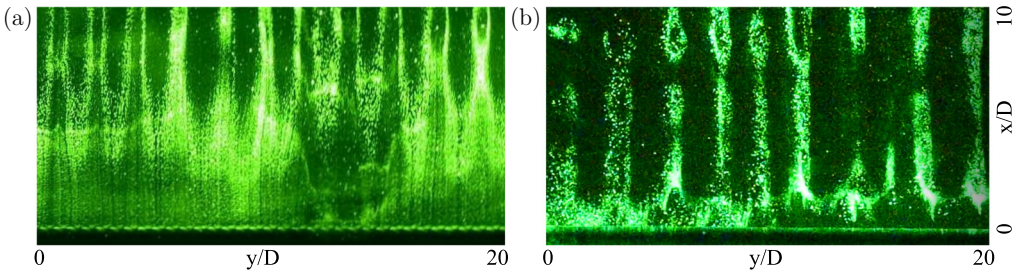

FIG. 5. Validation of the experimental setup for flow visualization in *xy* plane; (a) Radi *et al.* [31] (b) present experiment without wall. The flow is directed from bottom to top at Re = 250 and $\alpha = 2.1$. Scaling is same for both the images.

shedding downstream of the cylinder. Present experiments showed good agreement with the literature of Kumar *et al.* [17].

Validation of flow visualization experiments for spanwise study in the *xy* plane was done with Radi *et al.* [31]. All the modes reported in the literature were verified and Mode *E* at $\alpha = 2.1$ is shown in Fig. 5. Mode *E* is described when vortex shedding is suppressed in the *xy* plane at $\alpha \geqslant 2$. This mode originates from a stable wake and the spanwise wavelength of this mode is $\lambda/D \approx 2.1$. Present experiments showed good agreement with the literature of Radi *et al.* [31].

III. RESULTS AND DISCUSSION

This section discusses the effect of gap distance from the wall, Reynolds number, and forcing parameters (forcing frequency and oscillation amplitude) in the wake of the rotationally oscillating cylinder in the presence of a planar boundary. The experimental result consists of flow visualization data, hot-film measurements, and PIV data at Re = 250 and Re = 190, with subsequent qualitative and quantitative analysis. The present section also discusses the effect of gap distance, forcing frequency (FR), and forcing amplitude of oscillation, θ_0, on the three-dimensional (spanwise) structure of the wake of a rotationally oscillating cylinder in the presence of a plane wall at Re = 250. Spanwise modes (three-dimensionalities) in the wake are visualized, and their wavelength is quantified using image processing.

A. Effect of forcing parameters at $G/D = 0.5$

For the intermediate gap ratio of $G/D = 0.5$, the wall effect is significant for stationary cylinder wake, resulting in the flow asymmetry about the cylinder centerline (Fig. 6). Dipankar and Sengupta [13] showed that for a very small gap ratio, the upstream flow on the cylinder has large nonuniform shear which suppresses perturbations imposed by the cylinder. At this gap ratio of $G/D = 0.5$ (side closer to the wall), the planar wall boundary layer is also destabilized periodically by the vortices shed from the upper side (side toward the wall) of the cylinder. The shed vortex travels downstream parallel to the wall with a relatively constant convection velocity and stream-wise gap of 3–4D. The strong influence of the wall causes the flow to be asymmetric in the streamwise direction through the cylinder center. The shear layers from the top and bottom of the cylinder curl up into an alternating sequence of vortices of varying strength. Price *et al.* [1] showed that these vortices weaken the shear layer on the plane boundary downstream of the cylinder, instigating unsteady separation from the planar boundary near the vortex formation region in the wake of the cylinder. The flow separation phenomenon from the plane wall is mainly characterized by the adverse pressure gradient induced in the upstream and the downstream direction of the cylinder, as described in terms of a vortex-induced instability by Sengupta *et al.* [34] and Lim *et al.* [35]. Downstream of the cylinder, the existence of shed vortices generates an adverse pressure gradient which causes unsteady separation of the shear

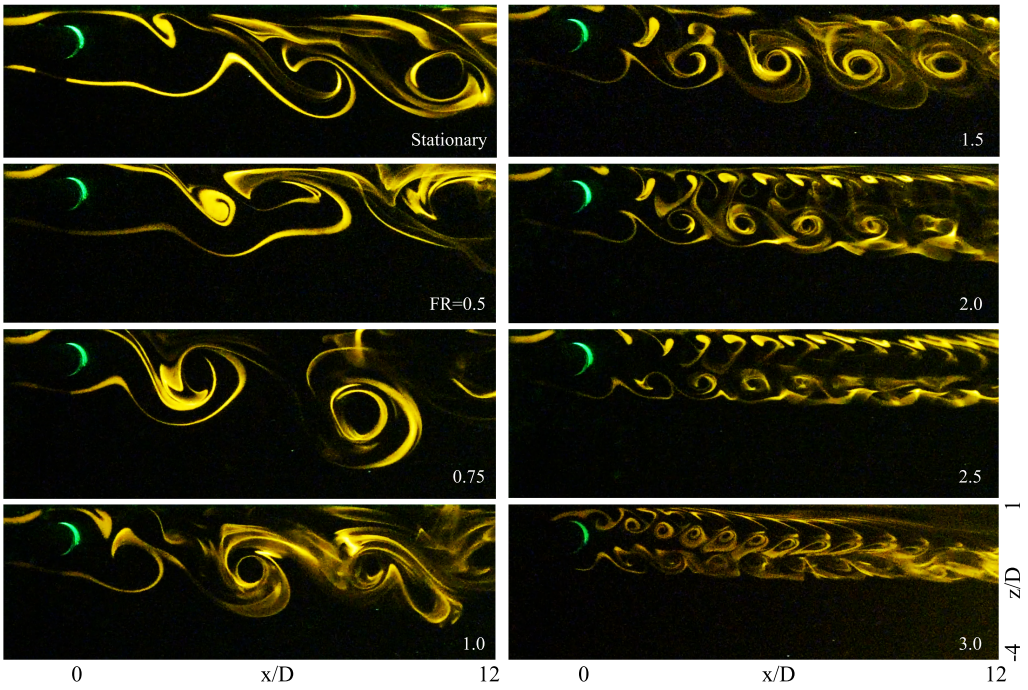

FIG. 6. Laser-induced fluorescence flow visualization at various FR for $G/D = 0.5$, $\theta_0 = \pi/2$ and Re = 250. Single-sided shedding occurs for FR $\leqslant 1$ and double-row vortices occur for FR > 1. Scaling is same for all the images.

layer from the planar boundary. Dipankar and Sengupta [13] also showed that the presence of shear in the upstream flow for a gap ratio of, $G/D = 0.5$, delays and weakens the shedding of vortices from the cylinder.

The interaction of the wall boundary layer with the vortices is such that the wall drives the vortices away from the streamwise direction through the cylinder center and a single layer vortex shedding is observed for FR $\leqslant 0.75$ at $\theta_0 = \pi/2$ and Re $= 250$ (as seen in Fig. 6). After FR $\geqslant 1.5$ double layer vortex street is observed comprising small-scaled vortices. This wake mode undergoes a change transitionally, with increasing FR, just as observed by Kumar *et al.* [17] for a stationary cylinder. These small-scale vortices merge to form a single-layer vortex downstream and as we increase FR, the downstream distance at which these vortices merge increases. These small-scale vortices, which are shed at higher frequencies of forcing at an oscillation amplitude of $\pi/2$, appear structurally similar to the shear-layer vortices which are formed by very small rotational oscillations as observed in the research of Filler *et al.* [36] and by small-amplitude oscillations laterally (Chyu *et al.* [37]; Chyu and Rockwell [38]). Shear-layer vortices, in a stationary cylinder, are not observed below Re ≈ 1100 (e.g., Wei and Smith [39]). The small-scale vortices shed downstream of the cylinder in the current experiment are locked onto the cylinder forcing frequency (checked by hot-wire anemometry), but they should not be mistaken for shear-layer vortices emerging due to the classical Kelvin-Helmholtz type of shear-layer instability because the frequencies of forcing are much more than the inherent shear layer frequency and the amplitude of oscillation are not as negligible as small perturbations. Figure 6 shows that the double-layer vortices start appearing at FR $= 1.5$ and become more prominent with increasing FR. At FR $= 3$, the shear layer from the wall gets influenced by the vortex shed from the cylinder such that the downstream wake appears to have a three-layer vortex shedding till 4D downstream. At $x/D \geqslant 4$ the shear layer from the wall merge with the vortices shed from the cylinder.

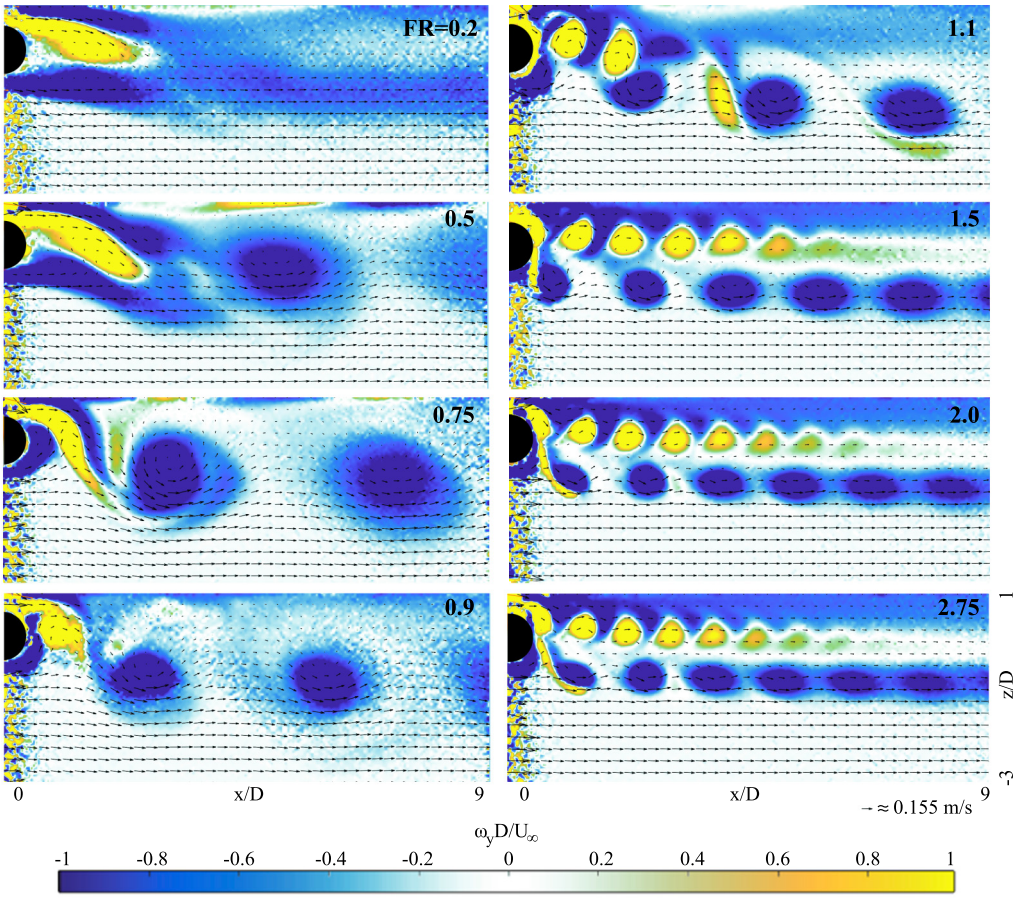

FIG. 7. Phase-locked time-averaged PIV (100 frames) in xz plane showing the velocity vectors and vorticity field at $\theta_0 = \pi/2$ and Re $= 250$. The wall is at the top end of all the images at $G/D = 0.5$. Vectors are five times scaled with every fifth vector plotted. Scaling is same for all the frames.

PIV data (time-averaged phase-locked data of 100 frames) showed that in the vicinity of the stationary cylinder (not shown here) or a cylinder at a very low forcing frequency of FR $= 0.2$ (see the first frame of Fig. 7), and the plane wall at $G/D = 0.5$, there are three shear layers as seen in the vorticity collage, the two shear layers that form along the cylinder's surface on the top and bottom, as well as the shear layer that develops along the wall. The lower shear layer on the cylinder has negative vorticity, and the upper shear layer on the cylinder has positive vorticity. The vortices emerging from the upper and lower shear layer of the cylinder attain maximum strength before they are shed. A shear layer of negative vorticity develops along the fixed wall downstream of the cylinder. Due to the boundary layer on the planar boundary, there is a strong secondary vortex. This wall-induced negative vortex interacts with the pair of vortices shed from the cylinder and strongly influences the shedding process. At the beginning of the shedding cycle, the induced vortex of negative sign at the upper shear layer develops rapidly before they are shed. This can be observed in the instantaneous PIV data at FR $= 0.2$ (not shown here) and not the mean image as the position of the shed vortex is at a different downstream location at different time instants at which the images were captured. The negative vortex shedding occurs from the cylinder at the side away from the wall (as seen in the frame FR $= 0.2$ of Fig. 7), and the induced positive vortex in the upper shear layer expands. The strong positive vortex induces a downward momentum and pushes the negative

vortex as it moves downstream. The upper shear layer is strongly influenced by the presence of the adjacent wall. The negative vortex on the wall shear layer grows and detaches from the wall. Near the wall, vorticity alters the sign further downstream of the cylinder as can be seen in Fig. 7 (yellow shear layer near the wall seen in the frames of FR = 0.5 and FR = 0.75). This indicates that a stagnation region exists near the wall for the cylinders at small forcing frequencies (see all the frames of FR $\leqslant$ 0.75). Fluid flowing below the cylinder separates from the front and produces a negative vortex. The upper face of the cylinder induces a positive vortex (as seen in Fig. 7, FR = 0.2). Downstream of the cylinder ($x/D = 2$), the flow separates. This separation seems to be periodically coupled with vortex shedding from the cylinder. Fluid is forced below after it impinges on the front of the cylinder. Fluid flowing below the cylinder is forced down behind the cylinder by the growing vortex on the cylinder's bottom surface. As the positive vortex originating from the cylinder's upper shear layer develops, a jet formation between it and the lower layer negative vortex takes place. This jet acts to propel fluid back toward the cylinder. A recirculation of flow occurs near the wall in the region downstream of the cylinder. This jet, through the gap between the wall and the cylinder, separates and does not curl up to form vortex shedding at small forcing frequencies. The separated lower shear layer of negative vorticity is almost horizontal at $G/D = 0.5$. The viscous effect decelerates the flow through the gap while the velocity of the flow on the bottom of the cylinder increases. The lesser the wall distance, the more extreme the viscous effect. As the cylinder frequency is not locked onto the vortex shedding frequency (checked by hot-film anemometry) at FR = 0.2, the time-averaged data of Fig. 7 does not reveal the vortices shed downstream of the cylinder (i.e., the vortices shed are not periodic).

For FR = 0.5, 0.75, and 0.9 (see Fig. 7) a vortex pair ready to move downstream emerges in the near wake. A negative vortex rolls up on the lower side of the cylinder. For FR = 0.5 (see Fig. 7), a set of three vortices comprising one vortex of positive sign from the upper side of the cylinder and two vortices of negative sign from the lower side of the cylinder and the plane wall is shed from the cylinder. Both, the generated vorticity from the upper side of the cylinder and the accelerated flow between the cylinder and the wall, are the reason for the growth of vorticity in the boundary layer on the planar boundary. Due to the interaction between the wake and the boundary layer, the vortex detaching from the upper side of the oscillating cylinder is stretched near the planar boundary by the vorticity of the opposite sign. While the initial negative vortex stays attached to the cylinder, a second negative vortex is produced, with the vortex induced on the plane wall. Near the wall at FR = 0.5, and FR = 0.75 (see Fig. 7), after a downstream distance of $x/D = 2.5$ and after the first vortex from the wall shear layer is shed, there are flat patches of alternate signed sheer layers that develop along the wall. For FR = 0.75 and 0.9, (see Fig. 7) the lower negative vortex is swept up and the positive vortex becomes more rounded in shape as compared to that of FR = 0.5 (see Fig. 7) where it was axially elongated. Subsequently, a pair of vortices with opposite signs form a narrow sheet, which is pushed by the jet from the gap to move away from the cylinder at an angle tilted away from the planar boundary. For these three forcing frequencies, the vortex-pair develops into a single vortex of negative sign as it moves downstream. The vortex of positive sign dissipates earlier (less downstream location) than the negative vortex, and eventually disappears so that only the negative vortex remains to form a single row of vortices of same-sign in the wake slightly further downstream from the cylinder. After FR = 0.9 (see Fig. 7), the shear layer patches that developed in lower forcing frequencies near the wall cease to exist. For FR = 1.5, double shear layer vortices are observed by Kumar *et al.* [17] for amplitude $\theta/2$ in the wake of the oscillating cylinder without the wall. With the wall present at $G/D = 0.5$ these vortices merge at a very near downstream location along with the negative vortex shed from the wall. The single negative vortex dominates the wake downstream and is shouldered by a small positive vortex. Increasing the frequency of forcing changes the mode shape in the near wake Williamson [23]. For FR = 2, 2.5, and 2.75 (see Fig. 7) the double layer vortices dominate the near wake region and negative vortices dominate after a downstream location of 5D where the positive vortices are nullified by the negative vortex below and the negative vorticity developed near the wall. The shear layer from the wall detaches at a downstream location of $x/D = 1.5$ and a shed vortex from the wall

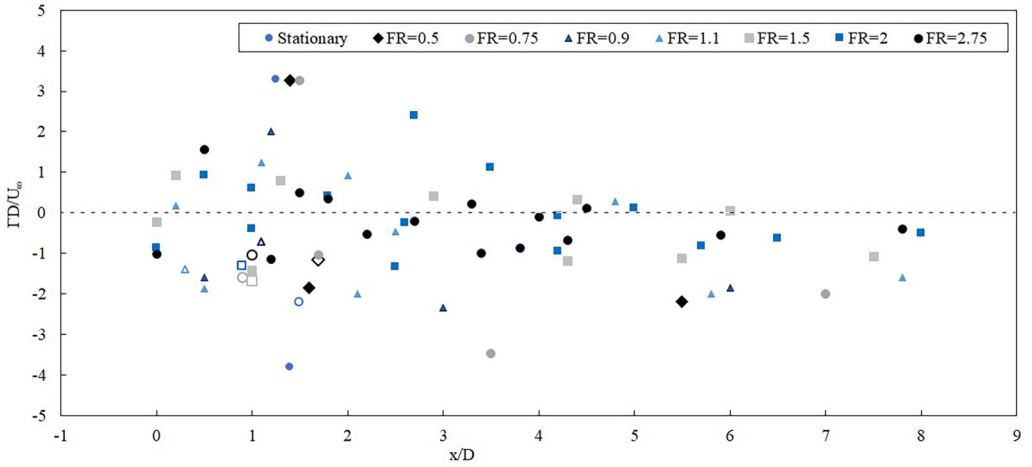

FIG. 8. Nondimensionalized circulation strength of the vortices (y axis) versus the downstream location of the area weighted centroid of the vortex (x axis) for various FR with oscillation amplitude of $\theta_0 = \pi/2$ at $G/D = 0.5$ and $\mathrm{Re} = 250$.

is formed. The size of the vortices shed also keeps decreasing with increasing forcing frequency and they become more compressed as seen in Fig. 7. The sizes of shed vortices from the upper and lower sides of the cylinder are not the same and the lower negative vortices are significantly bigger in size as compared to the positive vortices above.

The distribution of the magnitude of nondimensional circulation of the vortices at various downstream distances of the area-weighted centroid of the vortices obtained by phase-locked time-averaged PIV in the xz plane is shown in Fig. 8. There were more than sufficient number of vectors inside the vortex to resolve the circulation(i.e., more than eight unscaled vectors were there even to resolve the smallest of vortices). The centroid of the vortices denotes the average downstream location and the circulation magnitude of the vortex or shear layer at this location is plotted. The hollow marker in Fig. 8 shows the magnitude of circulation of the first shear layer shed from the wall. For a stationary cylinder, the time-averaged data reveals the recirculation shear layers near the cylinder and no downstream shed vortex. The magnitude of circulation of the shear layer in the stationary cylinder was found to be maximum as compared to the oscillating cases. For $\mathrm{FR} = 0.5$, $\mathrm{FR} = 0.75$, and $\mathrm{FR} = 0.9$, the positive shear layer has the maximum magnitude of circulation and the shed negative vortex has more magnitude of circulation as compared to the negative shear layer that develops from the cylinder and the wall. For $\mathrm{FR} \geqslant 1.1$ the shed positive vortex does not exist after a downstream distance of $x/D = 5$. The magnitude of circulation of positive vortices shed from the cylinder decrease with downstream distance and the magnitude of negative vortices increases with increasing downstream distance.

The effect of oscillation amplitude, as seen in Fig. 9, will be discussed for $G/D = 0.5$. At $\mathrm{FR} = 0.75$ [as seen in Fig. 9(a)], oscillation amplitude of $\theta_0 = \pi/4$ had a wake structure similar to the stationary cylinder. The vorticity flux from the surface of the cylinder is mainly because of the surface pressure gradient and tangential surface acceleration. The vorticity flux from the surface of the cylinder due to tangential surface acceleration is proportional to the amplitude of oscillation and the square of the forcing frequency. Hence, it becomes small at a lower amplitude independent of the forcing frequency although the vorticity flux, because of the effect of the pressure gradient, tends to a value appropriate for a stationary cylinder (Kumar *et al.* [17]). The present study revealed that the wake structure was more dependent on the forcing frequency rather than the oscillation amplitude for small forcing frequencies ($\mathrm{FR} \leqslant 1$). Figure 9(a) shows that at $\mathrm{FR} = 0.75$, the wake structure is almost similar for all oscillation amplitude. At an oscillation amplitude of $\theta_0 = \pi/2$,

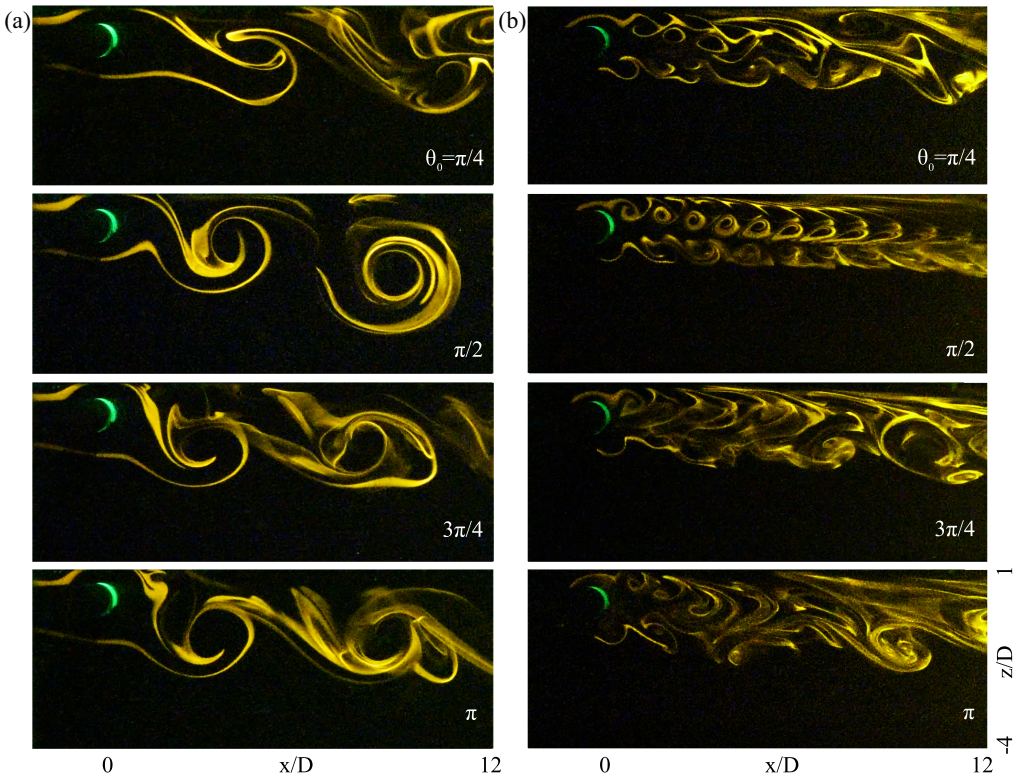

FIG. 9. Laser-induced fluorescence flow visualization at various oscillation amplitude, θ_0, for $G/D = 0.5$ and Re = 250 at a forcing frequency of (a) FR = 0.75, (b) FR = 2.75. Scaling is same for all the images.

it was seen that the vortices are more rounded in structure as compared to $\theta_0 = \pi/4$. Diffusion of the vortices was slightly more in the case of higher oscillation amplitude which may be attributed to centrifugal instability and higher mixing. At higher FR = 2.75, we saw that the combination of small-scale vortices shed from the cylinder to form pairs of larger vortices occurred nearer to the cylinder with an increase in oscillation amplitude from $\theta_0 = \pi/4$ to $\theta_0 = \pi$. These differences in the downstream distance where the vortex coalescence occurs may affect the lock-on parameter space (discussed in Sec. III D). The precise values of oscillation amplitudes at which the vortex-merger location alters its direction of motion was not explored in the present study.

Grass *et al.* [2] showed that the variation of St with G/D is highly dependent on the Reynolds number and that the Strouhal number is much more sensitive to G/D in the low Reynolds number range. The effect of the Reynolds number for the present experiment is such that the wake structure at Re = 150 appears brighter than the ones at Re = 190 and Re = 250 because of the lack of out-of-plane motion. This may be attributed to a two-dimensional flow at Re = 150. Figure 10 shows the effect of Re for the wake structure at $G/D = 0.5$. This suggests that axial flow in the near-field region or the out-of-plane motions occur at higher Re.

B. Effect of forcing parameters at $G/D = 1$

In the case of smaller gap ratios, as discussed for $G/D = 0.5$ in Sec. III A, the interaction between the two vorticity fields is strong, and the flow over the flat plate experiences unsteady separation in the vicinity of the cylinder. Such interactions commence as a result of the imposed adverse pressure gradient. This imposed adverse pressure gradient weakens with increasing the gap ratio and for

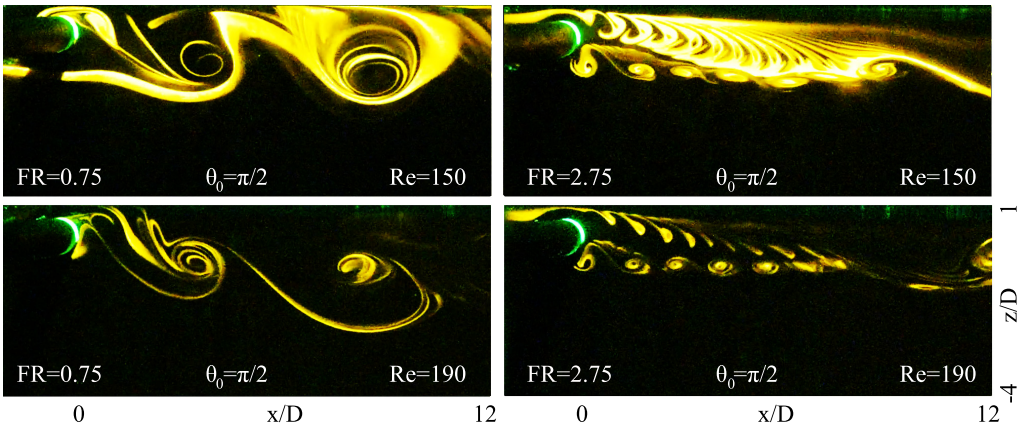

FIG. 10. Comparison of a rotationally oscillating cylinder wake for Re = 150 and Re = 190 at $G/D = 0.5$. Scaling is same for all the frames.

higher gap ratio cases the separation of flow from the cylinder is negligibly weak for a stationary cylinder (Dipankar and Sengupta [13]). Also, for $G/D = 0.5$ and FR = 0 cases, the cylinder may be exposed to an upstream shear flow which tends to weaken the vorticity shed from the upper half of the cylinder. In this case ($G/D = 1$), due to the increased gap distance between the cylinder and the planar boundary, the impressed pressure gradient generated by the stationary cylinder is weaker and the separation of flow on the planar boundary in the vicinity of the cylinder is minimal. Vortex-induced separation is observed downstream of the cylinder, as a result of the shed vortices, and is noticeable from the onset, appearing ahead of the shed vortex (as seen in Fig. 11). Furthermore, the size of the separation region reduces as G/D widens. As the flow accelerates through the gap between the cylinder and wall, it reattaches on the planar wall. There is no pairing between the wall shear layer and the shear layer that is shed from the upstream of the cylinder, unlike $G/D = 0.5$. At FR = 0.5 and 0.8, the flow pattern is almost like that of the stationary cylinder, however, at FR = 0.8 the flow is perfectly in a two-dimensional plane (xz plane) as the dye is not dissipated in the spanwise direction. The three-dimensionalities in the flow will be discussed in the subsequent section. The shear-layer shed from the bottom surface of the cylinder curls up in a periodic manner for the stationary cylinder as opposed to that at FR = 0.75. For all FR $\leqslant$ 0.8, the flow is directed away from the cylinder center-line toward the direction opposite to the side where the wall is present. With an increase in G/D, the exchange of momentum and spreading of wake decreases as compared to $G/D = 0.5$ where the effects of planar boundary proximity are considerable. Two shear layers shed from the cylinder at FR $\geqslant$ 1, as seen in Fig. 11, curl up in an alternating fashion producing a regular double-layer vortex shedding pattern. Downstream of the cylinder, alternate vortex shedding from the cylinder affects the planar wall boundary layer, causing it to separate in an aperiodic fashion at a frequency close to that of the vortex shedding (observed from hot-wire measurements). The vorticity induced by the boundary layer separation from the wall is in the opposite sense to that shed from the top of the cylinder similar to that of $G/D = 0.5$. This coupling between the wall boundary layer and the vortex shedding from the cylinder decreases as G/D increases. At FR = 1, the flow shows a characteristic feature of vortices shed from the upper and lower sides of the cylinder and the vortex street appears like a fish eye. The sizes of vortices shed from the upper and lower sides of the cylinder are different, and the vortices shed from the upper side move faster downstream than those shed from the lower side and they finally merge at 6D downstream. With an increase in the FR, at FR = 2 the merging occurs at a lesser downstream distance. At even higher FR = 2.75 the interaction of the wall boundary becomes negligible and the flow is almost similar to that of an isolated rotationally oscillating cylinder of Kumar *et al.* [17].

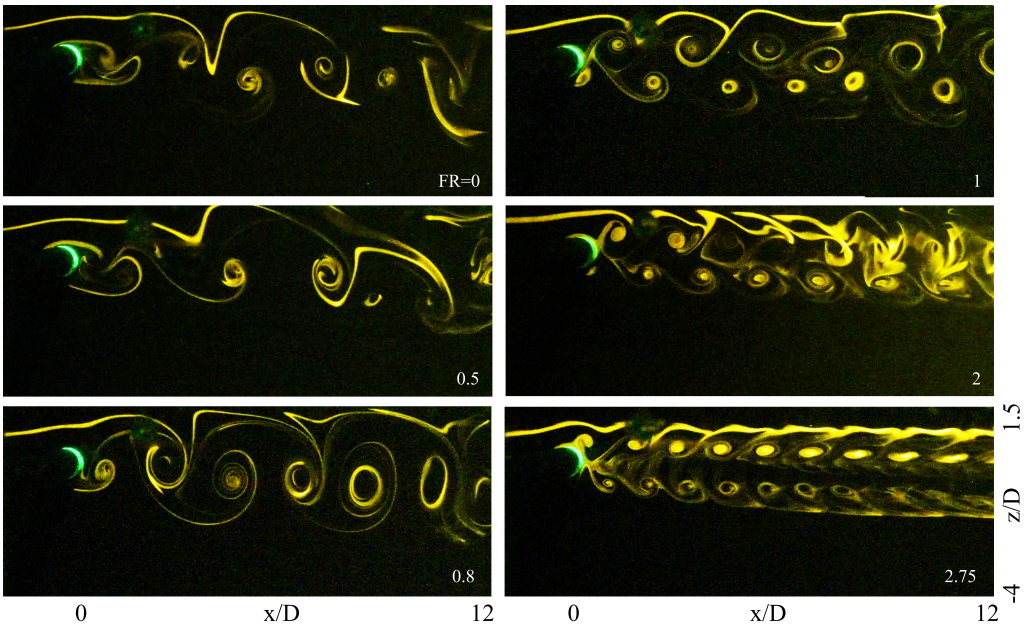

FIG. 11. Laser-induced fluorescence flow visualization at various FR for $G/D = 1$, $\theta_0 = \pi/2$, and Re = 250. Single-sided shedding occurs for FR < 1 and double-row vortices occur for FR $\geqslant 1$. Scaling is same for all the frames.

PIV data revealed that the initiation of nonsymmetry in the near wake is less pronounced as compared to $G/D = 0.5$. Figure 12 shows the phase-locked time-averaged PIV in xz plane at $\theta_0 = \pi/2$ and Re = 250. The presence of the shear from the planar wall causes the pair of vortices in the near wake of the stationary cylinder to move downward at an angle. Also, the positive vorticity appears as an extended vortex chain braided together, commencing from the upper part of the cylinder. It should be noted that in contrast to the suggestions of Taniguchi and Miyakoshi [40] and Grass *et al.* [2] the two shear-layers associated with the wall and the top of the cylinder, although of different sign vorticity, do not cancel each other out. The stationary cylinder wake is almost similar to that at $G/D = 0.5$. At a low FR = 0.5, the vorticity of flow is almost like that of the stationary cylinder. The shedding of the vortices is nonperiodic and hence the time-averaged data did not reveal the location of the shed vortices. This occurs because the cylinder oscillating frequency at this FR does not match the frequency of vortex shedding (i.e., the wake is not locked-on). At FR = 0.75 and FR = 0.9, the flow shows alternating shed vortices from the upper and lower edges of the cylinder. The positive vortex shoulders the negative vortex and because of the presence of the wall, the vortex pairs are drawn outward of the centerline with increasing downstream distance. The negative shear layer from the wall sheds and aids in to increase in negative vorticity of the vortex shed from the bottom of the cylinder. At FR = 1.5 and FR = 2.75 the double-layer vortices are seen which are shed downstream of the cylinder. The separation between the two rows of opposite sign vortices increases with an increase in frequency of forcing as visible in the near-field wake structures. The interaction of the wall shear layer is less as compared to $G/D = 0.5$. The positive vortices at the top half of the centerline are not canceled out by the negative vorticity from the wall and bottom half of the center line unlike in $G/D = 0.5$. At FR = 1.5, we observe that the strong negative sheer layer generated by the wall separates from the wall at $G/D = 6.5$ unlike the case at FR = 2.75 which might be attributed to the fact that the interaction of the boundary layer from the wall with the vortices shed from the cylinder weakens with an increase in FR in the range where double-row vortices are formed as the vortices with an increase in FR reduces in size. The downstream distance of the separation of

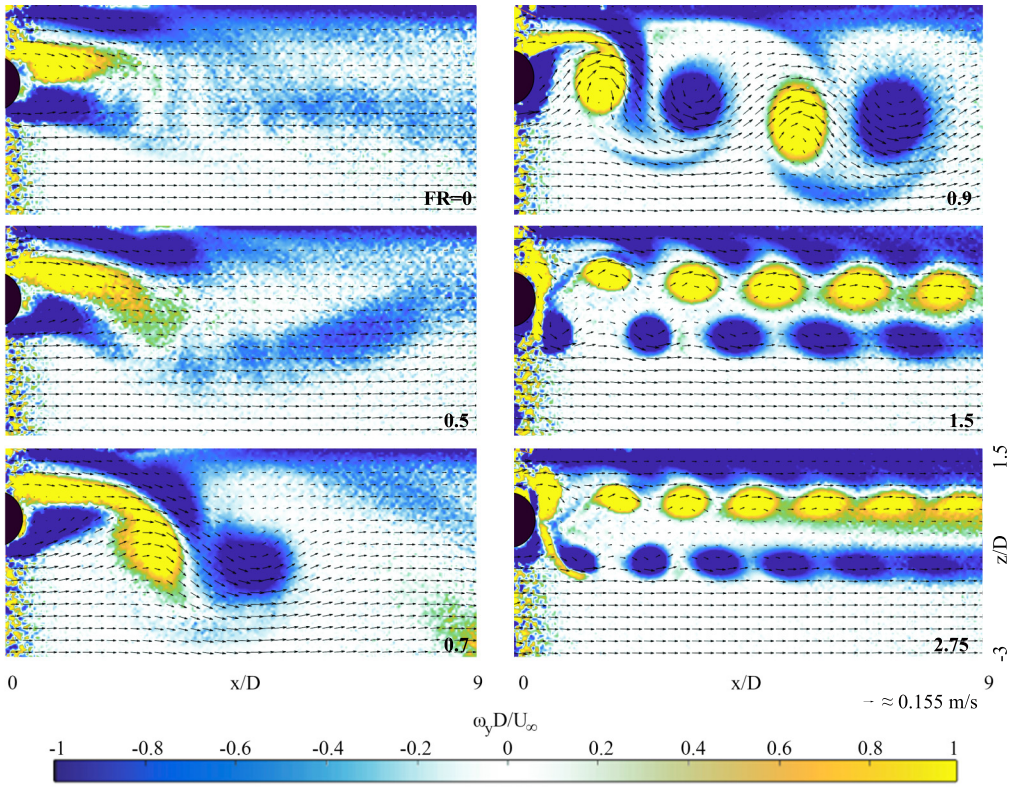

FIG. 12. Phase-locked time-averaged PIV (100 frames) in xz plane showing the velocity vectors and vorticity field at $\theta_0 = \pi/2$ and Re $= 250$ at $G/D = 1$. The wall is at the top end of all the images. Vectors are five times scaled with every fifth vector plotted. Scaling is same for all the frames.

a shear layer from the wall increases with increasing forcing frequency. The downstream distance at which the vortices merge increases with increasing forcing frequency. The vortices also flatten up with increasing frequencies of forcing. It was also observed that the downstream distance of the point of separation of the shear layer from the wall increases with increasing FR.

The distribution of the magnitude of nondimensional circulation of the vortices at various downstream distances of the area-weighted centroid of the vortices obtained by phase-locked time-averaged PIV in the xz plane for various forcing frequencies at $G/D = 1$ and Re $= 250$ is shown in Fig. 13. The hollow marker in Fig. 13 shows the magnitude of circulation of the first shear layer shed from the wall. For a stationary cylinder and $G/D = 0.5$, the time-averaged data reveals the recirculation shear layers near the cylinder and no downstream shed vortex. The magnitude of circulation of the wall shear layer was found to be more as compared to that of $G/D = 0.5$ (see Fig. 8) for a stationary cylinder. For FR $= 0.7$ and FR $= 0.9$, the positive shear layer has the maximum magnitude of circulation and the shed negative vortex has more magnitude of circulation as compared to the negative shear layer that develops from the cylinder and the wall. The maximum magnitude of circulation for the first shed vortices was found at a forcing frequency where the wake frequency (obtained from hot-wire measurements) begins to attain the frequency of the cylinder and the same phenomenon was observed by Kumar *et al.* [17] for an isolated rotationally oscillating cylinder. With a further increase in FR, the magnitude of circulation of first shed vortices decreases. For FR $\geqslant 1$ the shed positive vortex does not cease to exist unlike for $G/D = 0.5$. The shed positive vortices for FR $\geqslant 1$ is found to have almost a constant magnitude of circulation at $x/D \geqslant 3$ unlike for $G/D = 0.5$ where the magnitude of circulation of positive vortices shed from the cylinder

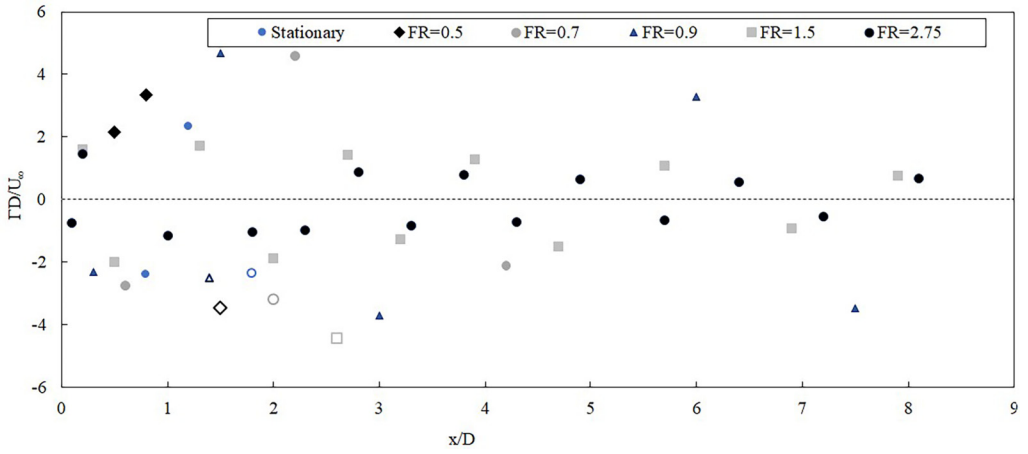

FIG. 13. Nondimensionalized circulation strength of the vortices (y axis) versus the downstream location of the area weighted centroid of the vortex (x axis) for various FR with oscillation amplitude of $\theta_0 = \pi/2$ at $G/D = 1$ and Re $= 250$.

decrease with downstream distance. The magnitude of negative vortices however decreases slightly with increasing downstream distance for FR $\geqslant 1$ which might be attributed to the fact that the negative vortices flatten with increasing downstream distance as observed in Fig. 8. The negative shear layer from the wall for the case of FR $= 2$ separates at a downstream distance of $x/D = 6$ and the magnitude of circulation of this wall shear is observed to be the maximum for the cases observed. For FR $= 2.75$, the negative shear layer from the wall does not separate before $x/D = 9$ and hence is not marked in Fig. 13.

The amplitude effect is only seen for $\pi/4$ (not shown here) at FR $= 2.75$, where the vortices merge earlier than at other amplitudes and are not affected by the wall when it is kept at $G/D = 1$. The wake structure is similar to the isolated cylinder case as observed by Kumar *et al.* [17]. The combination of small-scale shed vortices at higher forcing frequencies to form larger vortex pairs occurred closer to the cylinder with an increase in oscillation amplitude from $\pi/4$ to π. Figure 14 shows the effect of the Reynolds number for the wake structure at $G/D = 1$. For FR $= 2$ at

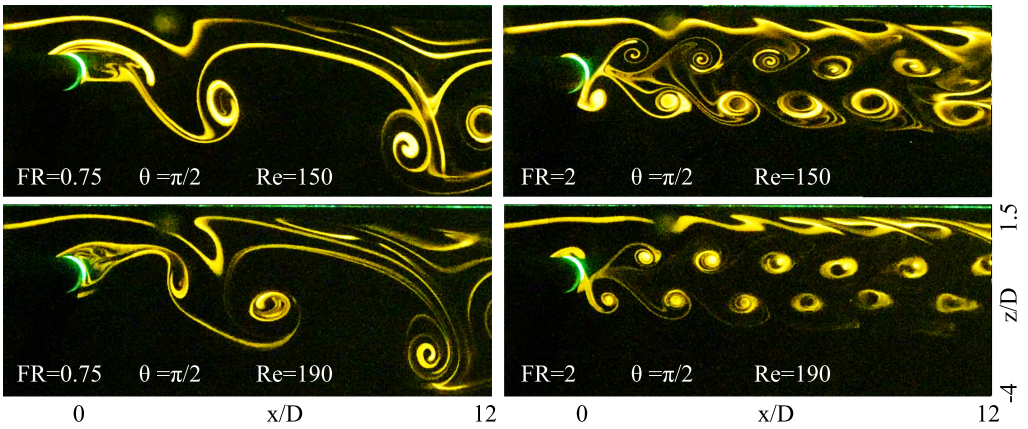

FIG. 14. Comparison of rotationally oscillating cylinder wake for Re $= 150$ and Re $= 190$ at $G/D = 1$. Scaling is same for all the frames.

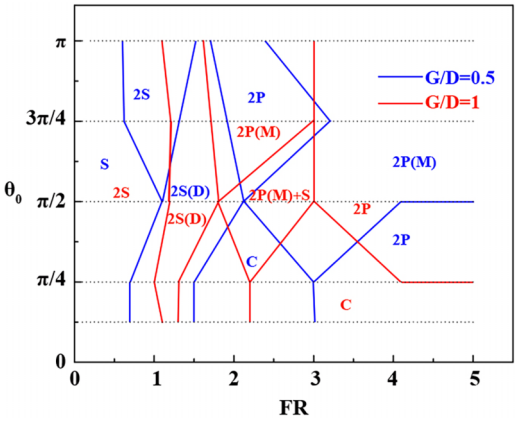

FIG. 15. Wake mode boundaries in the θ_0-FR parameter space for $G/D = 0.5$ (blue lines) and $G/D = 1$ (red lines) at Re $= 250$. The dots denote the test cases.

Re $= 190$, we observe three shear layer vortex shedding patterns. We observe that the wall shear layer is detached from the wall at 3D downstream. The visualization images at Re $= 150$ are brighter which may be attributed to the absence of three-dimensionalities. Due to a very large parameter space, several unique wake structures in the xz plane have been observed in the present investigation. In the present investigations, the rotational oscillation control has revealed a variety of possible wake modes and interactions. The wake modes and their boundaries in the frequency-amplitude plane are depicted in Fig. 15, and the terminology is consistent with that of Williamson and Roshko [41] for the two-cylinder wake modes as well as Sellappan and Pottebaum [5], where the wake modes of an isolated rotationally oscillating cylinder were discussed. These modes in the xz plane should not be confused with the three-dimensional modes in the xy plane discussed in Sec. III E. The dots in the figure denotes the test cases. Single-sided shedding in the near wake with one vortex shed per cycle is termed as "S." When a pair of vortices are shed per cycle like a deflected Kármán vortex street, it is termed as "2S." When double-row vortices start forming with a pair of vortices shed per cycle it is termed as "2S(D)." In one complete cycle, the inner shear layer vortices are alternately deflected and smeared out with the opposite outer shear layer vortices to create two vortices. The structure of the wake is of the double-row type, with a stagnation region forming between the rows. When two pairs of vortices are shed per cycle it is termed as "2P." This wake structure is observed over a wide range of frequencies and amplitudes. In this "2P" mode when the vortices from the upper and the lower half of the cylinder merge it is termed as "2P(M)." When the shear layer from the wall detaches and it appears like three sheets of vortices, the mode is termed as "2P(M)+S." Forcing conditions where unidentifiable and irregular patterns of wake are observed is termed as "C." This may be due to the abrupt coalescence of the vortices.

C. Effect of G/D

In the present experiments, it was found that the evolution and structure of the shear layers, in terms of wake width and flow curvature are different for various gap distances and forcing parameters. Figure 16 shows that the effect of the wall is more pronounced for low FRs as the width of the wake is more at lower FRs. For $G/D = 0.5$ the flow is similar to that for $G/D = 1$, except there is an even more prominent pairing between the top shear-layer shed from the cylinder and the wall boundary layer. For FR $= 0.75$ at $G/D = 0.5$, as seen in Fig. 16(a), we almost observe a single-sided vortex shedding with vortex shedding altered on the side of the cylinder where the wall is present. Karman-type vortex shedding is observed for $G/D = 1$ and $G/D = 2$ though the vortices are swept away from the centerline toward the opposite side of the wall. For $G/D = 3$, the cylinder

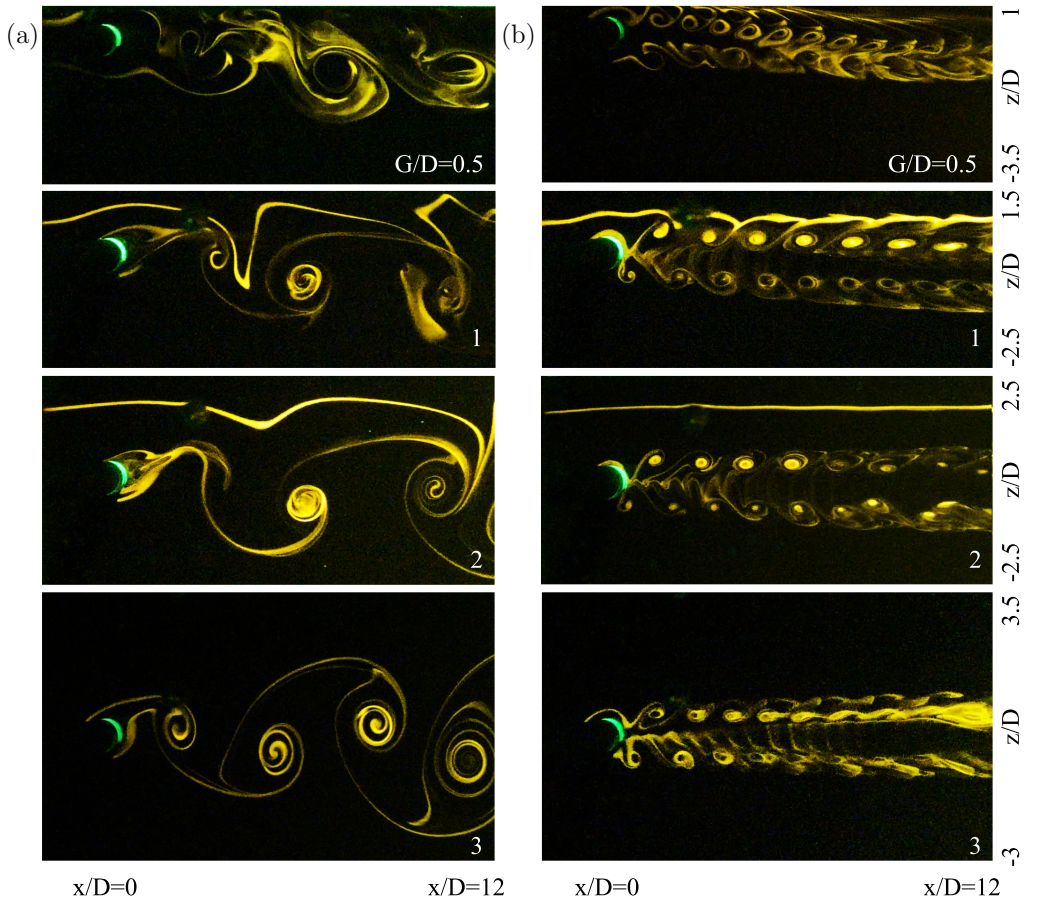

FIG. 16. Laser-induced fluorescence flow visualization for various G/D at Re $= 250$, and $\theta_0 = \pi/2$ with (a) FR $= 0.75$, (b) FR $= 2.75$. Scaling is same for all the frames.

behaves like an isolated cylinder and is virtually indistinguishable confirming the literature(Price *et al.* [1] and Cheng *et al.* [12]). The flow for $G/D = 3$ is symmetric to the z axis from the cylinder center-line for both low and high forcing frequencies. For FR $= 2.75$, as seen in Fig. 16(b), the wake behaves completely like an isolated cylinder at $G/D \geqslant 2$. At lower gap ratios of $G/D = 0.5$ and 1 double-layer vortex shedding is observed with the vortices being swept away from the centerline opposite to the wall. The wall boundary has a more significant effect on the vortices near it than the vortices on the other side. For $G/D = 0.5$, at FR $= 2.75$, it is observed that the wall induces the merger of the vortices shed from the top and the bottom of the cylinder at a near downstream location of $x/D = 5$. The boundary layer vortex from the wall and the counter-rotating vortex shed from the cylinder interact and result in vorticity annihilation via mixing. Suppression of vortex shedding which occurs for a stationary cylinder at $G/D \leqslant 0.3$ (Lei *et al.* [9]) is not observed for any of the studied forced conditions.

D. Wake-Frequency response

The frequency response of the wake to the forced rotary oscillation of the circular cylinder was studied using hot-wire anemometry with the fiber-film probe placed at $x/D = 4$ for various wall distances of $G/D = 1, 2, 3$ and ∞. It is observed that the shedding frequency and the St at a

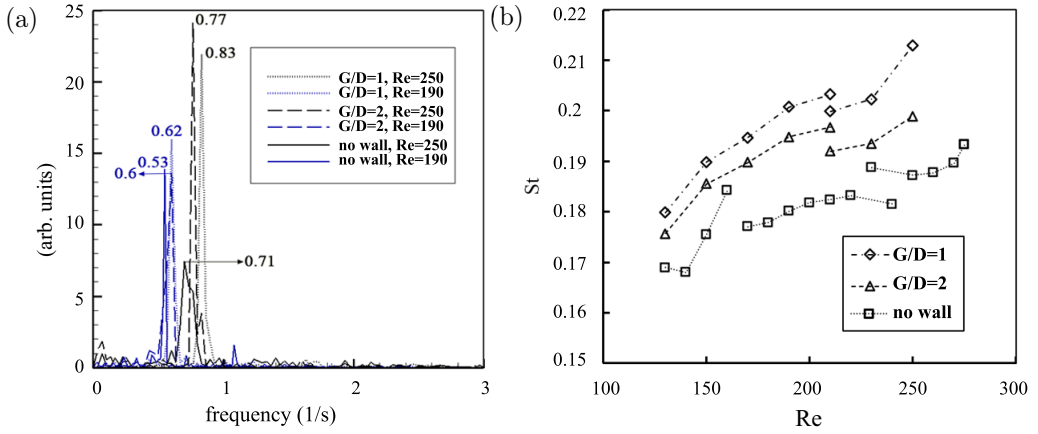

FIG. 17. Results from hot film anemometry for a stationary cylinder (FR = 0). (a) Spectral peak showing the shedding frequency. (b) Variation of St with Re at various gap ratios.

particular Re number increased with decreasing wall distance and the same is shown in Fig. 17. This effect of an increase in shedding frequency with decreasing gap ratio was also observed by Angrilli *et al.* [42]. Figure 17(a) shows the shedding frequency at various gap distances at a Re number of 190 and 250 for a stationary cylinder. The effect of the Re-St variation for a stationary cylinder at various gap ratios is shown in Fig. 17(b). The discontinuities in the plot [Fig. 17(b)] are because of the unstable Re regime in the wake where there is a transition of large-scale three-dimensionalities in the flow to small-scale three-dimensionalities (Williamson [23]). It should be noted that in the present experiments the influence of the upstream history and thickness of the boundary layer developing on the wall is not studied. When the boundary layer thickness is of the same order as the diameter of the cylinder, the Strouhal number depends on G/D (Bearman and Zdravkovich [8]). The effect of the upstream boundary layer is not a part of the present study. Subsequently, the effect of rotational oscillation of the cylinder on the frequency response of the wake is studied with a focus on lock-on, i.e., the frequency of the wake matching the cylinder oscillation forcing.

The power spectrum from the fiber-film probe was extracted for the five forcing oscillation amplitudes and the forcing frequency, FR ranging from 0 to 4 after which the lock-on parameter space was examined. Lock-on of the wake refers to the dominant frequency of the wake matching the cylinder oscillation frequency. Figure 18 shows representative data for lock-on for various forcing frequencies at Re = 190 and Re = 250 for the case of $G/D = 1$ and forcing amplitude of $\pi/2$. It is observed in Fig. 18(a) that there is only one dominant frequency at FR = 0 (stationary cylinder) which is the shedding frequency of the stationary cylinder for $G/D = 1$. Even at FR = 0.5 (frequency $f = 0.31$ Hz for Re = 190 and $f = 0.415$ Hz for Re = 250), as seen in Fig. 18(b), the cylinder wake is not locked on for both the Reynolds number and the dominating frequency is the still shedding frequency ($f_0 = 0.62$ Hz for Re = 190 and $f_0 = 0.83$ Hz for Re = 250). However, at FR = 0.75 ($f = 0.465$ Hz for Re = 190 and $f = 0.623$ Hz for Re = 250) and FR = 1.5 ($f = 0.93$ Hz for Re = 190 and $f = 1.245$ Hz for Re = 250), as seen in Figs. 18(c) and 18(d), it is found that the cylinder wake is exhibiting the lock-on phenomenon for both the Reynolds number. At FR = 2($f = 1.24$ Hz for Re = 190 and $f = 1.66$ Hz for Re = 250), as seen in Fig. 18(e), it is observed that the wake for the case of Re = 250 is locked on to the cylinder oscillation frequency (we see a peak at 1.66 Hz), whereas the case for Re = 190 (we do not see a peak at 1.24 Hz) is not exhibiting the lock-on phenomenon. Again, at FR = 3 ($f = 1.86$ Hz for Re = 190 and $f = 2.49$ Hz for Re = 250), as seen in Fig. 18(f), both the Reynolds number case showed that the wake was not locked on to the cylinder oscillation frequency. A similar power-spectrum was obtained for various ranges of FR, θ_0, and G/D (not shown here for preciseness) to obtain the lock-on parameter space.

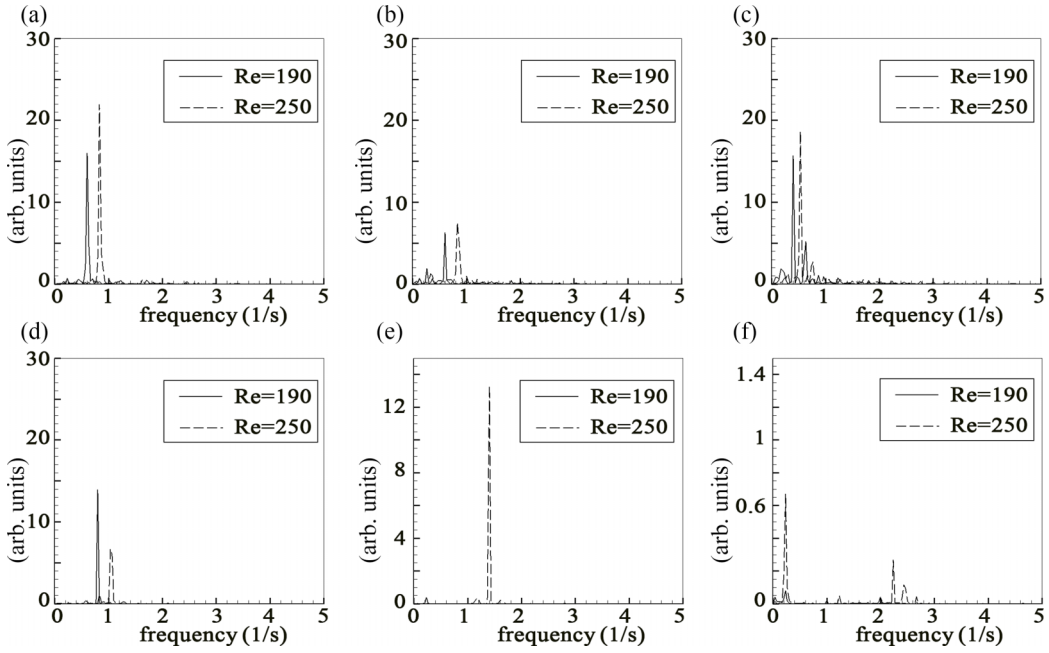

FIG. 18. Power-spectrum from hot-wire anemometry at $G/D = 1$, $\theta_0 = \pi/2$ for (a) FR = 0, (b) FR = 0.5, (c) FR = 0.75, (d) FR = 1.5, (e) FR = 2, (f) FR = 3.

The change in dominant frequency for the lock-on and non-lock-on regions are mainly attributed to the vortex merging process.

Hot-wire measurements showed the parameter space in which the vortices shed from the cylinder were locked onto the forcing frequency of the cylinder. This lock-on region was acquired from the spectrum of the stream-wise velocity fluctuations obtained by hot-film measurements at several forcing amplitudes studied in the current investigation. The data indicate that the existence of the wall and changes in the gap distance result in changes to the frequency response of the system and its synchronization with the downstream wake. Figure 19 shows for each forcing amplitude, at a downstream location of 4D, the lower and upper limits of the region of FRs where the dominant wake frequency is the same as the cylinder forcing frequency. The reason for the lock-on region significantly depending upon the oscillation amplitude may be attributed to the variability in the downstream location where the starting of new shedding mode due to the coalescence of the near-wake vortices occurs. Thiria and Wesfreid [18] were the first to predict through linear stability analysis that this variability possibly occurs due to changes in the mean flow stability characteristics near the cylinder. Lee and Lee [43] studied experimentally the flow past a rotationally oscillating cylinder at Re = 4140 (oscillation amplitudes,θ_0, ranging from 0 to $\pi/3$, and forcing frequency ratio, FR, varying from 0 to 2), and showed that lock-on always occurred at FR = 1 and that the lock-on region expanded with increasing amplitude. Figure 19 also shows that the low-frequency limits of the lock-on regions for almost all forcing amplitudes are near to each other for all gap ratios; however, the high-frequency limits show a considerable dependence on the gap ratio. It has been observed in the literature of Mahfouz and Badr [44], that below a limiting value of forcing amplitude there is no lock-on, i.e., the lock-on region diminishes to zero, but no such attempt was made in the present experiments to find this limiting value which is likely since it is much lower than the lowest forcing amplitude studied in the current experiments. Overall, it is seen that the lock-on parameter space reduces with a decrease in wall distance. It must be noted that at $G/D = 0.5$, measurements yielded irregular results, and, hence, it is not a part of the present discussion. The

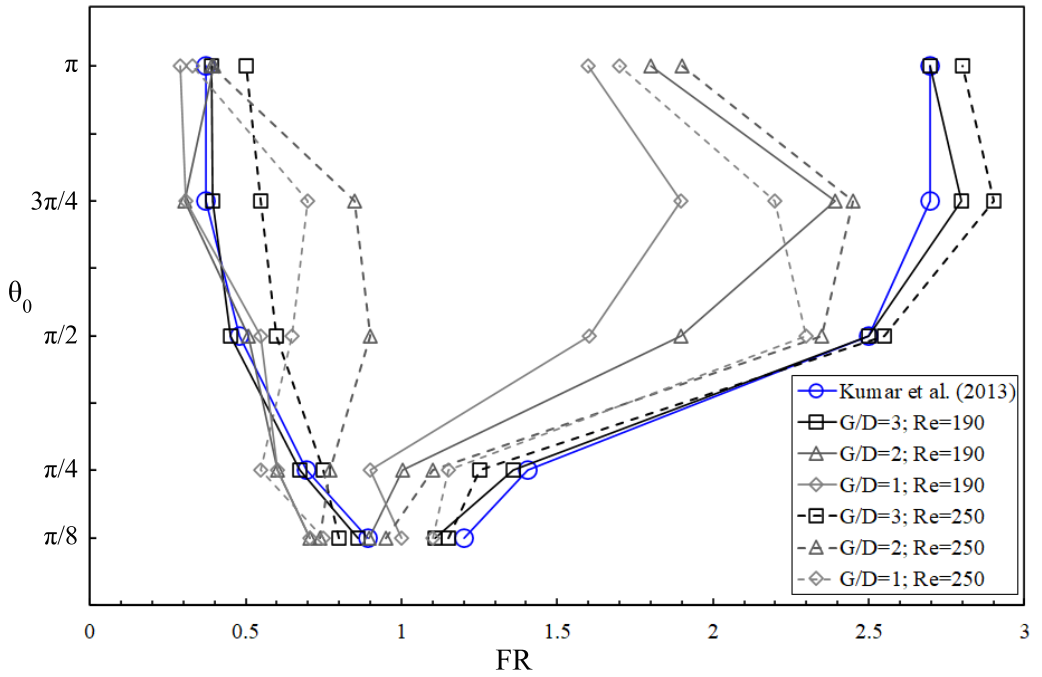

FIG. 19. Lock-on diagram: regions showing lock-on in the amplitude-frequency plane 4D downstream at various gap-ratios. The data points at five discrete amplitudes are joined by lines to show the parameter space of lock-on. The reference data from Kumar *et al.* [17] is for the unbounded case.

figure shows the effect of bringing the wall closer to the lock-on limits of a rotationally oscillating cylinder. The low FR limit of the lock-on diagram appears to move to the lower FRs as the wall is brought closer. It is also observed that the lock-on frequency range becomes wider as the forcing amplitude increases. Similar observations were also made by Kumar *et al.* [17] and Choi *et al.* [45]. The lock-on termination frequency reduces for $\theta_0 = \pi$. Similar observations were made by Kumar *et al.* [17] at $x/D = 2$ (not shown here) and the reason for the reduction of lock-on termination FR at high oscillation amplitude was cited as the coalescence of near-wake vortices. The data of Kumar *et al.* [17] in the unbounded domain is also shown in Fig. 19 since the case of gap ratio of $G/D = 3$ studied in the present work comes closest to their study, and the lock-on diagram almost approaches the case without the wall. Hence, at this gap ratio, the effect of the wall boundary layer with the cylinder vortices can be considered negligible at a downstream location of 4D. A similar observation was seen by Kumar [46] where a study was made for a rotationally oscillating cylinder inside variable channel boundaries. The overall, Re number effect was such that the lock-on mostly occurred at a slightly higher FR for Re = 250 than for Re = 190. This change can be attributed to the transition to three-dimensionality and mean flow stability characteristics near the cylinder (Thiria and Wesfreid [18]).

E. Three-dimensionalities in the flow

Three-dimensional flow visualization in the xy plane is performed using the hydrogen bubble flow technique. It is observed during the experiments that the best visualization was obtained when the wire was placed at an optimum distance from the xz symmetry plane. This distance varied with free-stream velocity and oscillation parameters, such that it had to be adjusted for each run. The stream-wise location of the wire was also varied for proper visualization of the vortices. Once the correct wire location was found, the three-dimensional modes could be visualized reliably. One

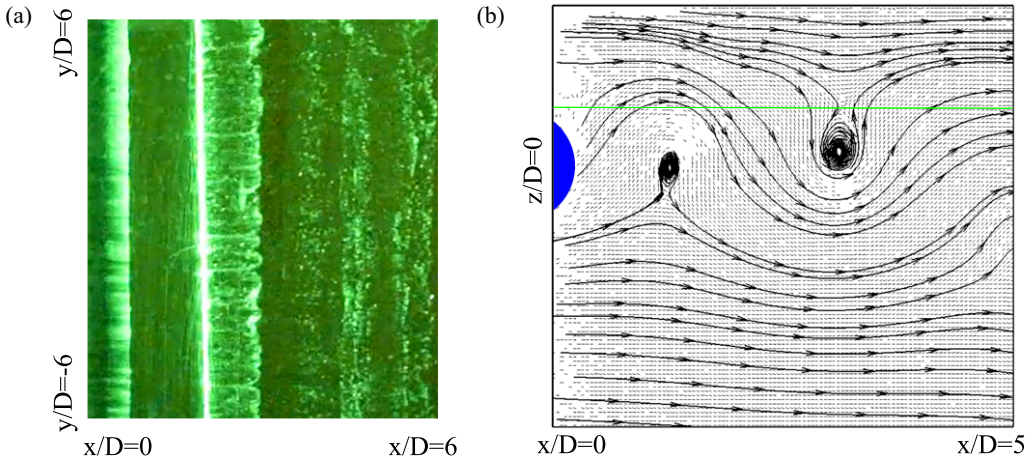

FIG. 20. Mode Z at FR $= 0.9$, $\theta_0 = \pi/2$, $G/D = 1$ and Re $= 250$: (a) hydrogen bubble flow visualization in xy plane; (b) streamlines obtained by synchronous instantaneous PIV in the xz plane. Green line denotes the plane in which panel (a) was obtained. Flow is directed from left to right.

major reservation regarding the application of qualitative hydrogen bubble flow visualization over extended streamwise domains (large downstream distance) is the streak line effect. Vortex stretching along with slow diffusion of the hydrogen bubbles as a passive scalar (Smits [47]), can lead to a misinterpretation of the existence of vorticity (Cimbala *et al.* [48]). Hence in our study, we focus only on a downstream distance of 6D where the streak line effect is negligible. The spanwise modes in the form of a hydrogen bubble sheet evolving from the platinum wire due to electrolysis are illuminated once they cross the laser sheet which is fired from the end of the cross-section. A similar technique of experimentation for finding three-dimensionalities in the downstream wake of a rotating cylinder and an isolated oscillating cylinder was applied by Radi *et al.* [31] and Bhattacharyya *et al.* [32,49], respectively.

The three-dimensional structures in the spanwise plane do not change with the wall distance for $G/D \geqslant 1$. The spanwise structures seen for cases without the wall are seen even with the presence of the wall. It is observed that these spanwise structures originate at a slightly reduced FR as we bring the plane wall closer to the cylinder. Mode B instability was visible (not shown here) with a characteristic wavelength of $\lambda/D \approx 1.18$ at Re $= 250$ for the stationary cylinder at all $G/D \geqslant 1$. At $G/D = 1$ and $G/D = 2$ increasing the forcing frequency to FR $= 0.5$ results in a flow that lacks spanwise coherence and intermittently changes structure. As the forcing frequency is increased to FR $= 0.85$, it appears that nonlinear interactions along the span are reduced as the resulting three-dimensional wake structure consists of a straight vortex column with a well-defined wavelength of $\lambda/D \approx 0.6$. The spatial-temporal coherence is very good, and the structure is repeatable. The bubble sheet enters the near wake and penetrates the laser sheet where it gets illuminated. At this location, the bubble sheet breaks up with one section moving downstream and the other slightly upstream for a small distance. The upstream moving part has oval cross-section vortices (braidlike formation) with a wavelength of $\lambda/D \approx 0.6$. This spanwise wavelength for a three-dimensional mode is obtained by spectral analysis. A similar analysis for obtaining the spanwise wavelength is discussed in detail by Bhattacharyya *et al.* [32]. This new mode is visible for all $\theta_0 \geqslant 4\pi/9$ and can be named Mode Z and is visualized in Fig. 20(a). Cross-stream movement of the platinum wire made this mode visible hence platinum wire is placed in a location where the three-dimensional patterns are visible. As suggested by Jacono *et al.* [33] this instability originates after the suppression of Mode A and Mode B three-dimensional modes and occurs when the near-wake transitions to a double-row shedding mode in the xz plane. Figure 20(b) shows the streamlines obtained by synchronous instantaneous

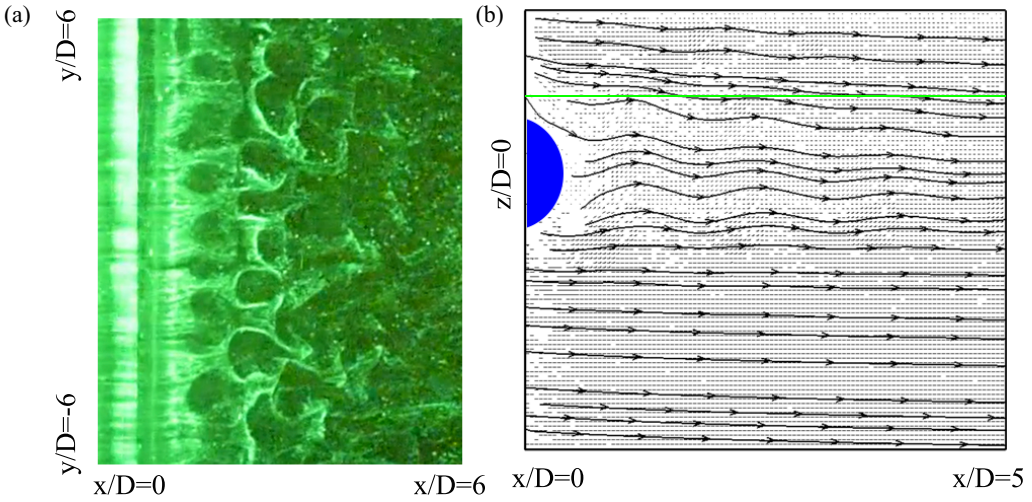

FIG. 21. Mode Y at FR $= 2.5$, $\theta_0 = \pi/2$, $G/D = 1$, and Re $= 250$: (a) hydrogen bubble flow visualization in xy plane; (b) streamlines obtained by synchronous instantaneous PIV in the xz plane. The green line denotes the plane in which panel (a) was obtained. Flow is directed from left to right.

PIV in the xz plane at $G/D = 1$. Although this mode is partially visible for $G/D = 0.5$ at a slightly lesser FR (FR $= 0.75$) the coherency of space and time is lost, and the flow almost appears two-dimensional.

There is an important observation made for $2.3 \leqslant \text{FR} \leqslant 2.75$ for $\theta_0 = 3\pi/4$ revealing a new mode with a cellular structure for $G/D \geqslant 1$ and the same is shown in Fig. 21(a). These structures are hexagonal and remain undistorted up to 6D downstream. The honeycomblike cells flatten up with an increasing downstream distance. The spanwise wavelength of this mode is $\lambda/D \approx 1.2$D. This mode remains unchanged from $1 \leqslant G/D \leqslant 3$. The flow visualization data for this mode is presented in Fig. 21(a) and this mode is named Mode Y. Hot-wire analysis performed by Bhattacharyya *et al.* [32] for an isolated cylinder showed the wake in this mode at $x/D = 2$ responds to the cylinder oscillation frequency but there are indications of the presence of multiple frequencies suggesting the complex behavior of this mode. The reason for this may be attributed to some instabilities occurring near the surface of the cylinder at these forcing conditions. Unlike the braid formation wrapping up the primary vortex in mode Z [Fig. 20(a)] the three-dimensionalities of this mode are primarily because of the shape of the span-wise counter-rotating vortices shed from the cylinder. Figure 21(b) shows the streamlines obtained by synchronous instantaneous PIV data in the xz plane. It must be noted that Figs. 20(a), 21(a), and 22 show spanwise flow up to a certain y/D, hence the interaction between the boundary developed from the tunnel's bottom and the vortex shedding of the cylinder is not seen.

The spanwise three-dimensional mode in the downstream wake of a rotationally oscillating cylinder in the presence of a planar boundary at $\theta_0 = 3\pi/4$ and FR $= 2.5$ are shown in Fig. 22. Figure 22(a) reveals the spanwise structures for the case of $G/D = 2$. The flow in Fig. 22 is directed from left to right. A distinct three-dimensional mode is seen where the spanwise vortices are well organized with time and space. This three-dimensional mode is suppressed for FR $\leqslant 2$ and FR $\geqslant 3.5$ and the flow is two-dimensional with the lack of spanwise structures at these forcing frequencies. Hence, these three-dimensional structures in the downstream wake are observed for a very narrow range of forcing frequencies. This three-dimensionality of the flow for an unbound rotationally oscillating cylinder with similar forcing conditions at Re $= 185$ was observed by Kumar *et al.* [17]. The three-dimensional wake vortices in the spanwise plane do not change with the wall distance for $G/D > 1$. The spanwise vortices seen for cases without the planar boundary are seen

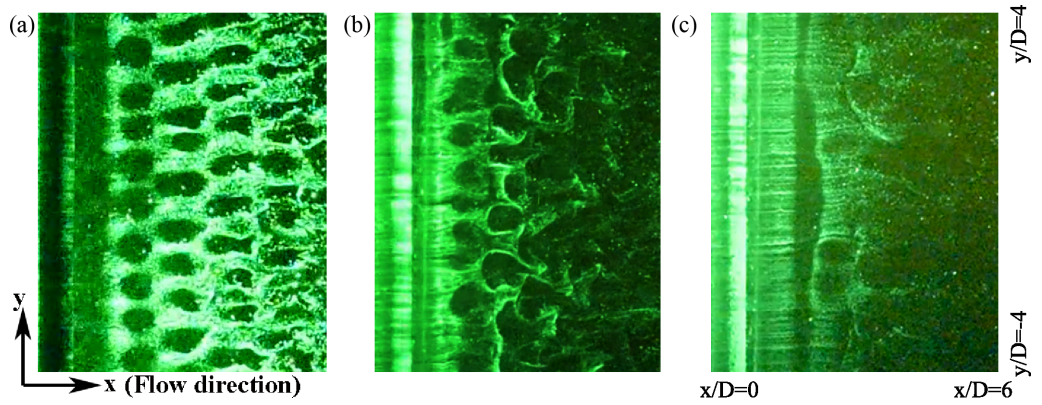

FIG. 22. Three-dimensional modes in wake of rotationally oscillating cylinder with a plane wall at $\theta_0 = 3\pi/4$ and FR = 2.5: (a) at $G/D = 2$; (b) at $G/D = 1$; (c) at $G/D = 0.5$. Platinum wire is not visible as it is 3D upstream of the cylinder. Flow is directed from left to right. The scaling is same for all the images.

even with the presence of the planar boundary for $G/D \geqslant 1$. However, for $G/D = 1$, the spanwise vortices are not as distinct as in the case of $G/D = 2$ and the same can be seen in Fig. 22(b). The vortices lack spatial-temporal coherency and are distorted. As the planar boundary is brought closer to the cylinder, at $G/D = 0.5$, the three-dimensionalities in the flow disappear and the flow almost becomes two-dimensional [see Fig. 22(c)]. Martinuzzi *et al.* [50] observed similar disappearance of three-dimensionalities in the flow for a square cylinder at $G/D \leqslant 0.7$.

IV. CONCLUSIONS

The results of water tunnel experiments on a rotationally oscillating cylinder in the presence of a planar boundary, for Re = 250 with various oscillation amplitudes and nondimensional forcing frequencies, are reported.

(1) LIF flow visualization showed that at certain cylinder forcing frequencies (FR $\leqslant$ 1) and wall gap distances ($G/D = 0.5$) the vortex shedding ceases on one side of the cylinder.

(2) Flow visualization and PIV at FR $\geqslant$ 2 and $G/D = 0.5$, showed that the positive shear layer shed from the cylinder gets canceled by the negative shear from the wall and the cylinder.

(3) At $G/D = 1$ the downstream distance at which the shear layer separates from the wall increases with increasing forcing frequency.

(4) Several unique wake structures in the xz plane have been observed in the present investigation and the rotational oscillation control has revealed a variety of possible wake modes and interactions. The wake modes and their boundaries in the frequency-amplitude plane are shown in Fig. 15.

(5) Hot-wire measurements revealed that the lock-on parameter space reduces with reducing gap distance and with an increase in oscillation amplitude the forcing frequency for lock-on increases.

(6) The three-dimensional study using hydrogen bubble flow visualization confirmed new modes Mode Z and Mode Y with a spanwise wavelength of $\lambda \approx .75$D and $\lambda \approx 1.5$D respectively. It is observed that three-dimensionalities in the flow for Mode Y reduces (only partially occurs along the span) with reducing gap distance.

ACKNOWLEDGMENTS

The authors acknowledge the support provided by Grant No. ARDB/01/1031875/M/I from Aeronautics Research and Development Board (ARDB), DRDO (India).

[1] S. Price, D. Sumner, J. Smith, K. Leong, and M. Paidoussis, Flow visualization around a circular cylinder near to a plane wall, J. Fluids Struct. **16**, 175 (2002).
[2] A. J. Grass, P. W. J. Raven, R. J. Stuart, and J. A. Bray, The influence of boundary layer velocity gradients and bed proximity on vortex shedding from free spanning pipelines, J. Energy Res. Technol. **106**, 70 (1984).
[3] C. D. Bridge, H. A. Howells *et al.*, Observations and modeling of steel catenary riser trenches, in *Proceedings of the 17th International Offshore and Polar Engineering Conference* (International Society of Offshore and Polar Engineers, Mountain View, CA, 2007).
[4] I. B. Ivshina, M. S. Kuyukina, A. V. Krivoruchko, A. A. Elkin, S. O. Makarov, C. J. Cunningham, T. A. Peshkur, R. M. Atlas, and J. C. Philp, Oil spill problems and sustainable response strategies through new technologies, Environ. Sci.: Process. Impacts **17**, 1201 (2015).
[5] P. Sellappan and T. Pottebaum, Vortex shedding and heat transfer in rotationally oscillating cylinders, J. Fluid Mech. **748**, 549 (2014).
[6] I. H. Khan, P. Sunil, S. Bhattacharyya, R. Yadav, K. Poddar, and S. Kumar, Flow past two rotationally oscillating cylinders, J. Fluid Mech. **969**, A16 (2023).
[7] S. Taneda, Experimental investigation of vortex streets, J. Phys. Soc. Jpn. **20**, 1714 (1965).
[8] P. W. Bearman and M. M. Zdravkovich, Flow around a circular cylinder near a plane boundary, J. Fluid Mech. **89**, 33 (1978).
[9] C. Lei, L. Cheng, and K. Kavanagh, Re-examination of the effect of a plane boundary on force and vortex shedding of a circular cylinder, J. Wind Eng. Ind. Aerodyn. **80**, 263 (1999).
[10] C. Lei, L. Cheng, S. Armfield, and K. Kavanagh, Vortex shedding suppression for flow over a circular cylinder near a plane boundary, Ocean Eng. **27**, 1109 (2000).
[11] M. Zdravkovich, Forces on a circular cylinder near a plane wall, Appl. Ocean Res. **7**, 197 (1985).
[12] M. Cheng, H. E. Tsuei, and K. L. Chow, Experimental study on flow interference phenomena of cylinder/cylinder and cylinder/plane arrangements, ASME-Publications-PVP **273**, 173 (1994).
[13] A. Dipankar and T. Sengupta, Flow past a circular cylinder in the vicinity of a plane wall, J. Fluids Struct. **20**, 403 (2005).
[14] M. Cheng and L.-S. Luo, Characteristics of two-dimensional flow around a rotating circular cylinder near a plane wall, Phys. Fluids **19**, 063601 (2007).
[15] N. G. Chikkam and S. Kumar, Flow past a rotating hydrophobic/nonhydrophobic circular cylinder in a flowing soap film, Phys. Rev. Fluids **4**, 114802 (2019).
[16] B. Thiria, S. Goujon-Durand, and J. Wesfreid, The wake of a cylinder performing rotary oscillations, J. Fluid Mech. **560**, 123 (2006).
[17] S. Kumar, C. Lopez, O. Probst, G. Francisco, D. Askari, and Y. Yang, Flow past a rotationally oscillating cylinder, J. Fluid Mech. **735**, 307 (2013).
[18] B. Thiria and J. Wesfreid, Stability properties of forced wakes, J. Fluid Mech. **579**, 137 (2007).
[19] X.-Y. Lu and J. Sato, A numerical study of flow past a rotationally oscillating circular cylinder, J. Fluids Struct. **10**, 829 (1996).
[20] P. Sunil, S. Kumar, and K. Poddar, Flow past a rotationally oscillating cylinder with an attached flexible filament, J. Fluid Mech. **930**, A3 (2022).
[21] C. H. K. Williamson, Vortex dynamics in the cylinder wake, Annu. Rev. Fluid Mech. **28**, 477 (1996).
[22] A. Roshko, On the drag and shedding frequency of two-dimensional bluff bodies, National Advisory Committee for Aeronautics Technical Note **3169**, 509 (1954).
[23] C. Williamson, The existence of two stages in the transition to three-dimensionality of a cylinder wake, Phys. Fluids **31**, 3165 (1988).
[24] J. Dušek, P. L. Gal, and P. Fraunie, A numerical and theoretical study of the first Hopf bifurcation in a cylinder wake, J. Fluid Mech. **264**, 59 (1994).
[25] D. Barkley and R. D. Henderson, Three-dimensional Floquet stability analysis of the wake of a circular cylinder, J. Fluid Mech. **322**, 215 (1996).
[26] M. Thompson, K. Hourigan, and J. Sheridan, Three-dimensional instabilities in the wake of a circular cylinder, Exp. Therm Fluid Sci. **12**, 190 (1996).

[27] H. Zhang, U. Fey, B. R. Noack, M. König, and H. Eckelmann, On the transition of the cylinder wake, Phys. Fluids **7**, 779 (1995).
[28] J. Wu, J. Sheridan, M. C. Welsh, and K. Hourigan, Three-dimensional vortex structures in a cylinder wake, J. Fluid Mech. **312**, 201 (1996).
[29] T. Leweke and C. Williamson, Three-dimensional instabilities in wake transition, Eur. J. Mech. B Fluids **17**, 571 (1998), special issue Dynamics and Statistics of Concentrated Vortices in Turbulent Flow (Euromech Colloquium 364).
[30] A. Rao, J. Leontini, M. C. Thompson, and K. Hourigan, Three-dimensionality in the wake of a rotating cylinder in a uniform flow, J. Fluid Mech. **717**, 1 (2013).
[31] A. Radi, M. C. Thompson, A. Rao, K. Hourigan, and J. Sheridan, Experimental evidence of new three-dimensional modes in the wake of a rotating cylinder, J. Fluid Mech. **734**, 567 (2013).
[32] S. Bhattacharyya, I. H. Khan, S. Verma, S. Kumar, and K. Poddar, Experimental investigation of three-dimensional modes in the wake of a rotationally oscillating cylinder, J. Fluid Mech. **950**, A10 (2022).
[33] D. L. Jacono, J. S. Leontini, M. C. Thompson, and J. Sheridan, Modification of three-dimensional transition in the wake of a rotationally oscillating cylinder, J. Fluid Mech. **643**, 349 (2010).
[34] T. K. Sengupta, S. De, and S. Sarkar, Vortex-induced instability of an incompressible wall-bounded shear layer, J. Fluid Mech. **493**, 277 (2003).
[35] T. Lim, T. Sengupta, and M. Chattopadhyay, A visual study of vortex-induced subcritical instability on a flat plate laminar boundary layer, Exp. Fluids **37**, 47 (2004).
[36] J. Filler, P. Marston, and W. Mih, Response of the shear layers separating from a circular cylinder to small-amplitude rotational oscillations, J. Fluid Mech. **231**, 481 (1991).
[37] C. Chyu, J.-C. Lin, J. Sheridan, and D. Rockwell, Kármán vortex formation from a cylinder: Role of phase-locked Kelvin–Helmholtz vortices, Phys. Fluids **7**, 2288 (1995).
[38] C. Chyu and D. Rockwell, Near-wake structure of an oscillating cylinder: Effect of controlled shear-layer vortices, J. Fluid Mech. **322**, 21 (1996).
[39] T. Wei and C. Smith, Secondary vortices in the wake of circular cylinders, J. Fluid Mech. **169**, 513 (1986).
[40] S. Taniguchi and K. Miyakoshi, Fluctuating fluid forces acting on a circular cylinder and interference with a plane wall, Exp. Fluids **9**, 197 (1990).
[41] C. H. Williamson and A. Roshko, Vortex formation in the wake of an oscillating cylinder, J. Fluids Struct. **2**, 355 (1988).
[42] F. Angrilli, S. Bergamaschi, and V. Cossalter, Investigation of wall-induced modifications to vortex shedding from a circular cylinder, J. Fluids Eng. **104**, 518 (1982).
[43] S.-J. Lee and J.-Y. Lee, Flow structure of wake behind a rotationally oscillating circular cylinder, J. Fluids Struct. **22**, 1097 (2006).
[44] F. Mahfouz and H. Badr, Flow structure in the wake of a rotationally oscillating cylinder, J. Fluids Eng. **122**, 290 (2000).
[45] S. Choi, H. Choi, and S. Kang, Characteristics of flow over a rotationally oscillating cylinder at low Reynolds number, Phys. Fluids **14**, 2767 (2002).
[46] S. Kumar, Effect of channel inlet blockage on the wake structure of a rotationally oscillating cylinder, J. Fluids Eng. **138**, 121203 (2016).
[47] A. J. Smits and T. T. Lim, *Flow Visualization: Techniques and Examples* (World Scientific, Imperial College Press, Singapore, 2012).
[48] J. M. Cimbala, H. M. Nagib, and A. Roshko, Large structure in the far wakes of two-dimensional bluff bodies, J. Fluid Mech. **190**, 265 (1988).
[49] S. Bhattacharyya, I. Hussain Khan, P. Sunil, S. Kumar, and K. Poddar, Experimental investigation of flow past a rotationally oscillating tapered cylinder, Phys. Rev. Fluids **8**, 054103 (2023).
[50] R. J. Martinuzzi, S. C. C. Bailey, and G. A. Kopp, Influence of wall proximity on vortex shedding from a square cylinder, Exp. Fluids **34**, 585 (2003).